NASA CR-168,282

NASA Contractor Report 168282

NASA-CR-168282
19840008078

POTENTIAL FLOW ANALYSIS OF GLAZE ICE ACCRETIONS ON AN AIRFOIL

Ronald J. Zaguli

The Ohio State University
Columbus, Ohio

January 1984

LIBRARY COPY

LANGLEY RESEARCH CENTER
LIBRARY, NASA
HAMPTON, VIRGINIA

Prepared for

NATIONAL AERONAUTICS AND SPACE ADMINISTRATION
Lewis Research Center
Under Grant NAG3-28

TABLE OF CONTENTS

N84-16146 #

NOMENCLATURE

a_{MN}, b_{MN}	Influence coefficients, Eq.(6)
c	Airfoil chord length
Cd	Airfoil drag coefficient
C_ℓ	Airfoil lift coefficient
$C_{\ell MAX}$	Airfoil maximum lift coefficient
Cm	Airfoil moment coefficient
Cp	Pressure coefficient
d	Droplet diameter, microns
k	Roughness height
K	Number of distributed vortices
ℓ	Panel length
LWC	Liquid water content, g/m
M	Mach number
P	Local static pressure, Eq.(9)
P_∞	Free stream static pressure
Re	Reynolds number
t	Time of icing encounter, minutes
T	Temperature, C
u,v	Velocity in X,Y directions induced by a vortex, Eq.(3)
$\bar{u},\bar{v}$	Net velocity in X,Y directions induced by all vortices, Eq.(4)
$\tilde{u}$	Total fluid velocity, Eq.(11)

U_∞	Free stream velocity
$V_{N_{ip}}$	Prescribed normal velocity at panel midpoint
X,Y	Horizontal, vertical coordinates
Xo,Yo	Coordinates of vortex center
α	Angle of attack, degrees
α_{STALL}	Stall angle of attack, degrees
ε	Local panel abscissa
γ_p	Parabolic vorticity factor
Γ	Vortex strength
ϕ	Velocity potential, Eq.(2)
ρ	Air density
ρ_{ice}	Ice density, g/cm
σ	Source strength, Eq.(13)
θ	Local surface slope

I. INTRODUCTION

> Ice is an insidious enemy. It attacks on two flanks, adding weight to the airplane and at the same time ruining its aerodynamic shape. As ice accumulates, more and more power is necessary to maintain speed and altitude, and the pilot gradually finds himself forced to sacrifice first his speed and then bit by bit his altitude in a desperate struggle to stay airborne [1].

The effects of ice growth on the performance of an aircraft are felt primarily through aerodynamic penalties; a drastic reduction in $C_{\ell MAX}$ and α_{STALL} and an increase in drag. The two classes of ice accretions, known as rime and glaze, are formed under different flight conditions. Rime ice is formed at low air temperatures and low velocities. The droplets freeze on impact and usually are found in flight through clouds with low liquid water content. Figure 1 shows an example of a rime ice accretion with its characteristic streamlined leading edge.

Glaze ice on the other hand is formed at temperatures near the freezing mark and higher velocities. With this type of ice growth, a phenomenon known as runback occurs. Rather than freezing on impact, the water droplets travel a short distance before freezing. The resulting shapes are of the type shown in Figure 1, with the characteristic horns. It is with glaze ice accretions that the greatest aerodynamic losses are found, and it is this type of ice that is the subject of this paper.

Classically, most of the work done in the study of icing, particularly that done by the NACA in the 1950's, was concerned with mechanical means of preventing or removing the ice, known as anti- or de-icing. However, with the increase in general aviation aircraft with smaller powerplants and lighter weight, a mechanical method of solving the ice problem is no longer acceptable. Retro-fitting the aircraft components with pneumatic boots or heating elements tend to increase the aircraft's weight, cost, and complexity.

A better approach would be to design the component itself with characteristics that would reduce the chances of ice growth and the detrimental effects if growth does occur. This process has been investigated by Bragg [2,3,4] for rime accretions but no attempt has been made for glaze ice conditions. Gray [5,6] derived an empirical formula for predicting iced airfoil performance degradation but the correlation has not been found to fit recent experimental data very well.

When trying to develop a method for evaluating the glaze ice problem, two phases must be examined. The first, a thermodynamic problem, deals with the prediction of the actual geometry of the ice shape. The second is to determine a scheme for analyzing the performance losses incurred once the geometry of the ice has been determined. The study described in this paper applies current potential flow methods to this problem. The approach discussed is not a final solution to the problem. Rather, it is intended as a first step in developing a glaze ice analysis method. Further investigation into the properties of the flowfield in the region of the ice accretion is required before a complete scheme can be formulated.

II. SURVEY OF LITERATURE

Most of the early investigations into the icing phenomenon were concerned with de-icing. The first of these efforts was the development of inflatable de-icing boots by the B.F. Goodrich Company in the 1930's. This concept is still in wide use today. Refinements have reduced the boot in its deflated form to the point that its presence barely affects the geometry of the wing.

The first major investigation into the icing characteristics of various airfoils and the resultant aerodynamic penalties was performed by the NACA in the 1950's [5]. Information was gathered on the 65A004, 63A009, 0011, 65-212, and 63-015 airfoils. However, few correlations were drawn between the aerodynamic penalties incurred and the shape and location of the ice accretion.

The first major effort to draw these correlations was by Vernon Gray [5,6] in the 1960's at the Lewis Research Center. Gray developed an empirical equation which relates known icing conditions with change in drag coefficient. The major testing was performed in the NASA Lewis 6' x 9' Icing Research Tunnel on the NACA 65A004 airfoil. A wide range of parameters were examined, including icing time, airspeed, freestream temperature, liquid water content, cloud droplet impingement efficiency, angle of attack and leading edge radius of curvature. However, the correlation he developed from this study does not readily predict changes in lift coefficient and moment coefficient. An interesting facet of Gray's correlation is the ability to mathematically grow the ice at a given angle of attack and then study the performance changes at another angle. Recent data however has shown that even though Gray's correlation reasonably predicts ΔCd at the angle the ice is grown, its accuracy drops significantly when the calculation is performed at another angle of attack.

Some interesting observations by Laschka and Jesse [7] came from other investigations in the Lewis Icing Tunnel. They observed that as the angle of attack is varied, many different ice shapes will be obtained. Also they noted that when the time of the icing encounter, t, is varied, the ice height will be approximately proportional to the value of t, while the impingement limits are time independent.

In order to begin quantifying the performance degradation due to ice, a scheme had to be developed which could predict the flowfield about the irregular ice shape. In 1968, Dvorak published a method to predict the development of turbulent boundary layers over rough surfaces [8]. This approach is incorporated in his program, which was investigated in this paper.

In addition to the roughness effects associated with icing, is the existence of a large separation bubble in the area of the ice shape. Little research has been done studying these laminar separation bubbles. Most computer programs, such as the Eppler code [9], when they predict laminar separation, consider this simply a transition point between laminar and turbulent boundary layers. However Venkateswarl and Marsden [10] investigated laminar separation bubbles that occur at 60-70% chord. They developed a correlation to predict the size and shape of the laminar bubble. Also in 1976, Crimi and Reeves [11] studied leading edge laminar separation bubbles and developed a scheme to predict the onset of transition in the shear layer.

In the late 70's and the present, icing research has increased with the work of Ingelman-Sundberg, Shaw, Bragg, Gregorek and others. Ingelman-Sundberg and Trunov [12] published a joint report from the Swedish-Soviet Working Group on Scientific-Technical Cooperation in the Field of Flight Safety. Flight test and icing wind tunnel studies were performed and the concept of simulated ice was developed as a means of investigating the aerodynamic effects of ice growths.

Shaw [13], Bragg and Gregorek [2,3,4] continued investigation in the Lewis Icing Research Tunnel in the 1980's. Extensive data were collected on the lift and drag penalties of ice growths. Rime and glaze ice accretions were modelled using mahogany and pressure tapped so detailed aerodynamic data could be collected. This work serves as the primary database for the analytical effort to be presented in this paper.

Of particular importance to the glaze ice analysis was the work of Pfeiffer and Zumwalt [14] and McLachlan and Karancheti [15] who investigated the flowfield around airfoils with highly deflected spoilers. Pfeiffer and Zumwalt utilized a splitter plate arrangement to visualize the separated zones created by the spoiler.

Lastly, Bristow [16] has developed an inviscid computer program which allows for input of mixed analysis/design boundary conditions. For example, the input to the program can consist of an airfoil with its geometry partially defined and a desired pressure distribution in the undefined region. The program will then hold the input geometry fixed and design the remaining portion of the airfoil based on the input pressures. This program was particularly useful in the author's investigation of the separation zone associated with glaze ice.

This review of literature should give the reader a clear picture of the deficiency of direct investigations into the glaze ice problem. It is hoped that the study reported here will spawn continued efforts in this area.

III. POTENTIAL FLOW THEORY AND PANELLING METHODS

In order to analyze the performance degradation that occurs due to glaze ice accretions, a method for predicting the flowfield and therefore the pressure distribution of the iced airfoil must be developed. As a first step in accomplishing this task, current potential flow computer programs were investigated. These potential flow solutions are based on an incompressible, inviscid, and irrotational fluid, for which the classical Navier-Stokes Equation can be reduced to the Laplace Equation,

$$\nabla^2\phi = 0 \qquad (1)$$

One scheme presently in use to solve this equation involves the distribution of surface singularities on a closed polygon which approximates the airfoil contour. This method is known as panelling. Examples of computer programs using this technique are; 1) Smetana, by F. Smetana, D. Sumney, N. Smith, and R. Carden [17]; 2) Eppler, by R. Eppler and D. Somers [9]; 3) Dvorak, by F. A. Dvorak and F. A. Woodward [8]; and 4) Bristow, by D. R. Bristow [16]. The potential flow method of each of these programs will be discussed in this chapter.

Smetana

The Smetana program approximates the airfoil geometry by a closed polygon. Vortices are placed on the perimeter of the polygon (Figure 2). The velocity potential for each of these vortices can be expressed by:

$$\phi = \frac{\Gamma}{2\pi} \tan^{-1} \frac{Y-Yo}{X-Xo} \qquad (2)$$

where Γ is the vortex strength and (Xo,Yo) is the location of the center of the vortex. This potential satisfies Laplace's Equation, which is linear and therefore the sum of any number of these potentials also will be a solution. The corresponding velocity expressions can be obtained by differentiation of the potential:

$$u = \frac{\partial\phi}{\partial X} = \frac{-\Gamma}{2\pi} \frac{Y-Yo}{(X-Xo)^2+(Y-Yo)^2}$$

$$(3)$$

$$v = \frac{\partial\phi}{\partial Y} = \frac{\Gamma}{2\pi} \frac{X-Xo}{(X-Xo)^2+(Y-Yo)^2}$$

The contributions of each vortex to the net velocity at a point (X,Y) can then be treated separately and summed. Therefore, the net velocity components, $\bar{u}$ and $\bar{v}$, are:

$$\bar{u} = \frac{-1}{2\pi} \sum_{N=1}^{K} \frac{(Y-Yo_N)\ \Gamma_N}{(X-Xo_N)^2+(Y-Yo_N)^2}$$

$$\bar{v} = \frac{1}{2\pi} \sum_{N=1}^{K} \frac{(X-Xo_N)\ \Gamma_N}{(X-Xo_N)^2+(Y-Yo_N)^2} \tag{4}$$

where K is the total number of vortices and (Xo,Yo) is the location of the center of the Nth vortex.

The boundary condition that must be satisfied is that the flow must be parallel to the airfoil surface. Adding the contribution of the freestream velocity to the velocity components induced by the vortices, this condition can be written:

$$\frac{\bar{v}}{U_\infty+\bar{u}} = \left(\frac{dY}{dX}\right)_{wing} - \tan\alpha \tag{5}$$

If we denote the right side of this equation as B_M and define

$$a_{MN} = \frac{(Y_M-Yo_N)}{(X_M-Xo_N)^2+(Y_M-Yo_N)^2}$$

and (6)

$$b_{MN} = \frac{(X_M-Xo_N)}{(X_M-Xo_N)^2+(Y_M-Yo_N)^2}$$

we can write Equation (5) as,

$$B_1 = \frac{b_{11}\Gamma_1 + b_{12}\Gamma_2 + \ \ldots \ + b_{1K}\Gamma_K}{2\pi U_\infty + a_{11}\Gamma_1 + a_{12}\Gamma_2 + \ \ldots \ + a_{1K}\Gamma_K}$$

$$\bullet$$
$$\bullet$$
$$\bullet \qquad (7)$$
$$\bullet$$

$$B_K = \frac{b_{K1}\Gamma_1 + b_{K2}\Gamma_2 + \ \ldots \ + b_{KK}\Gamma_K}{2\pi U_\infty + a_{K1}\Gamma_1 + a_{K2}\Gamma_2 + \ \ldots \ + a_{KK}\Gamma_K}$$

This set of equations is then solved for the needed values of the vortex strength, Γ.

The influence coefficients a_{MN} and b_{MN} are solved for convenience at the midpoints of each panel. However, from the geometry, only K-1 values of the coefficients can be calculated unless the polygon is closed. The trailing edge point is then given two indices, N=1 and N=K. Then the system is determinant and can be easily solved.

To satisfy the Kutta condition at the trailing edge, Smetana chose

$$\Gamma_1 = -\Gamma_K \qquad (8)$$

which still satisfies the requirement that the circulation at the trailing edge is zero. Since the trailing edge was denoted by the indices N=1 and N=K, the net vortex strength at the trailing edge is $\Gamma_1 + \Gamma_K = 0$. Thus Equation (7) contains K-1 distinct values of Γ_N and K-1 values of B_M and is therefore solvable.

Lastly, in order to obtain surface pressures, Smetana uses the equation:

$$P = P_\infty - \frac{1}{2} \rho \ (\bar{u}^2 + \bar{v}^2 + 2\bar{u}U_\infty) \tag{9}$$

which is derived from the Bernoulli equation:

$$P_T = P_S + \frac{1}{2} \rho \tilde{u}^2 \tag{10}$$

where $\tilde{u}$ is the total fluid velocity and is calculated using the vector magnitude formula:

$$\tilde{u} = \sqrt{(U_\infty + \bar{u})^2 + \bar{v}^2} \tag{11}$$

<u>Eppler</u>

The Eppler program is very similar in construction to the Smetana code in that both utilize vortices to provide circulation and both satisfy the same flow tangency boundary condition. However, the Eppler code satisfies it on the actual input geometry points. Also, rather than applying a point vortex, Eppler distributes the vortices parabolically along each airfoil panel. The geometry of the panels is determined by a cubic spline fit of the input coordinates. The vortex strengths at the endpoints of each panel are solved for in the same manner as

Smetana.

The vorticity distribution between the panel endpoints is obtained from the equation:

$$\Gamma(\varepsilon) = \frac{\varepsilon}{\ell}\left(1 - \frac{\varepsilon}{\ell}\right)\gamma_p \qquad (12)$$

where ℓ is the length of the panel, ε is the local panel abscissa, and γ_p is a parabolic vorticity factor. This factor is calculated using the vortex strengths at the endpoints of the two surrounding panels. Integration of the vortex distribution is then required to evaluate the velocity contributions of each panel.

The Kutta condition is satisfied as in the Smetana program. The requirement again is equal velocities on both sides of the trailing edge and zero normal velocity with respect to the trailing edge bisector angle. Thus, enough circulation is generated that the trailing edge becomes the rear stagnation point.

Dvorak

The airfoil contour is again represented by an inscribed polygon. However each pair of adjacent panels has a triangular distribution of vorticity across it. The airfoil is thus modelled by a series of overlapping triangular vortex distributions. At the leading edge of the airfoil, the strength of the upper and lower surface vortices are set equal to insure smooth flow.

The Kutta condition is satisfied by setting the strengths of the vortices on the trailing edge panels equal to zero. However, doing this reduces the system of equations to be solved to N equations with N-1 unknowns. An additional unknown is added by applying a constant source distribution on the inside of the airfoil surface. It should be pointed out that like the vortex strength of the trailing edge point used by Smetana and Eppler, this unknown source strength is always very nearly zero for airfoils with closed trailing edges.

Bristow

The Bristow code is similar in design to Smetana and Eppler, however the singularities used on each panel are linear source and vortex distributions associated with the classical third identity of Green. One of the particular advantages of this method is believed to be its high numerical stability when used in the design mode of operation.

The vortex distribution generated is linear on each panel and the source distribution can be either piecewise constant or linear. This choice however shows little effect on the results obtained. The source strength at panel midpoints, σ_i , is found simply from the following equation:

$$\sigma_i = V_{N_{i_p}} + U_\infty \sin (\theta_i - \alpha) \qquad (13)$$

where $V_{N_{i_p}}$ is the prescribed normal velocity at the panel midpoints and θ_i is the local slope. With the prescribed source strength evaluated, it is left only to determine the total potential at a panel midpoint induced by the simultaneous action of the vortex and source distributions.

The Bristow code has a unique feature. It can perform mixed analysis-design problems. The user inputs fixed geometry regions and the desired surface velocities in the design region. The program immediately satisfies surface continuity by stretching the input starting geometry in the design region. Then an analysis only solution is obtained from the combined source-vortex singularity scheme. The geometry of the design region is then modified using a first order inverse method to minimize the difference between calculated and input values of tangential and normal velocities. This process is repeated until the convergence criterion is met.

Laminar Separation Bubbles

One cannot deal with glaze ice accretions solely using potential flow methods. This is due to the presence of a laminar separation bubble which forms behind the glaze ice horn. Short laminar separation bubbles have very little effect on the integrated aerodynamic loads and most computer analysis programs assume that the bubble simply represents a transition point from laminar to turbulent boundary layers. However, laminar bubbles of the type seen with ice accretions are sufficiently large that their effect cannot be neglected.

Most of the work done on laminar separation bubbles has been of an experimental nature. This is due to the difficulty in analyzing the interaction between the viscid and inviscid flow in the reverse flow region inside the bubble. In addition, evaluation of the transition point from laminar to turbulent flow in the free shear layer becomes more complicated.

A diagram of a typical flow pattern observed with a separation bubble is shown in Figure 3. The laminar boundary layer first separates from the surface yielding the region of reverse flow. Transition to turbulent flow occurs in the separated shear layer shortly before reattachment. The region is divided by the streamline which separates from the surface and reattaches downstream. The area below the separation streamline is known as the recirculation region or separation bubble.

Most of the examinations into the problem of laminar separation bubbles have used the classical boundary layer assumption that

$$\frac{\partial P}{\partial Y} = 0 \qquad (14)$$

From Schlichting [18] however, it is noted that this term is of the order of the boundary layer thickness. For most cases, this would be a valid assumption. However, the bubble behind a glaze ice accretion is much thicker than normal boundary layers and therefore the assumption that this term can be neglected may not be valid. In Chapter 5, the order of magnitude of this term is investigated.

In an effort to analyze these separation bubbles using potential flow schemes, the assumption that the pressure gradient term is negligible will be considered valid. Pressures measured experimentally at the airfoil surface will be input to the Bristow code in the design mode. The corresponding calculated bubble shape will then be compared with the flow visualization results.

IV. EXPERIMENTAL PROGRAM

Very little experimental data has been available on the performance degradation of airfoil sections resulting from ice accretions. To help alleviate this, a two-year test program was conducted in the NASA Lewis 6' x 9' Icing Research Tunnel(IRT-Figure 4). Its primary objectives were:

1). To examine a method of simulating ice accretions with wood shapes which were instrumented with surface pressure taps to obtain aerodynamic data.

2). To study and document the complex flowfield in the region of the ice shape through pressure distributions and flow visualization techniques.

3). To expand the current database of performance data on airfoils under icing conditions [4,19].

The first tunnel entry in 1981 was an actual ice accretion study. Glaze and Rime ice shapes were grown on a 1.36 m chord NACA 63A415 model. The resulting section drag coefficients were measured using a wake survey probe. Two flight regimes were examined during the test; 1) cruise, with high velocity and low angle of attack, and 2) climb, with low velocity and high angle of attack. The temperature in the tunnel was set to -4 degrees C to generate glaze ice shapes and -26 degrees C for rime shapes.

Two methods are available for recording the ice accretion geometry. For short icing times, a small section of ice is scraped away near the leading edge of the model. A template is then inserted into the gap and a tracing can be made. For longer periods of accretion, a section of the ice is removed by spraying steam inside the model near the leading edge. It is then dipped into a container of molten beeswax. After hardening, the water is removed, the plaster is poured inside and casts are then available for more detailed tracings [13].

From the shapes generated during this tunnel entry, 2 rime and 2 glaze shapes were chosen to represent typical climb and cruise conditions. These shapes were then modelled for the second tunnel entry. Table 1 gives a summary of the pertinent test parameters which generated the chosen shapes.

TABLE 1

Ice Generation Test Parameters

TYPE	T	α	U_∞	d	LWC	t	ρ_{ice}
RIME	-26	2.6	51	15	1.5	15	0.421
RIME	-26	6.6	40	15	1.5	15	0.534
GLAZE	-4	2.6	51	15	1.5	15	-----
GLAZE	-4	6.6	40	20	2.9	15	-----

A fifth shape, denoted Generic Glaze was derived from the work of Ingelman-Sundberg [12]. This shape was chosen because it readily scales down to a 6" chord model. Comparison testing of this shape will be performed in the Ohio State Transonic Wind Tunnel Facility.

The simulated ice shapes were formed from mahogany and extended full span. In order to obtain surface pressures, the inside of each shape was hollowed out to allow clearance for the 1/8" ID tubing required for tapping (Figures 5-7).

In order to obtain pressures on the airfoil itself, 1/8" OD strip- a-tube was attached to the surface. In order to simulate the natural roughness of ice accretions, aluminum oxide grit with a k/c=.00058 was attached using an acrylic spray adhesive to the glaze shapes, while a grit with a k/c=.0012 was added to the rime shapes.

Data acquisition and reduction was accomplished using the OSU Digital Data Acquisition and Reduction System (DDARS) [20]. The heart of the system (illustrated in Figure 8) is a DEC LSI-11 microcomputer. System input and output is through a standard teletype terminal, and the mass storage device is a single-head dual-drive floppy disc. Signals from the various pressure transducers and the wake probe slidewire enter the analog front-end, which conditions the signal and converts it into digital format for direct input to the microcomputer.

A Scanivalve transducer system was used to provide surface pressures on the model and a twin-head wake survey probe, with wake total and static ports, was used to sample pressures in the wake. Drag data were then obtained using the wake momentum deficit technique. Figure 9 shows a schematic of the data acquisition system set-up.

One of the key features of the OSU DDARS is on-line data reduction. The system operator is given quick-look Cp distributions as well as integrated values of C_ℓ, Cm, and Cd. The engineer can then evaluate the progress of the test and maximize tunnel usage time.

Final data reduction was performed on the OSU Harris/6 Computer System. Hard-copy plots of the Cp distributions for each configuration were generated and integrated values of lift, moment, and drag coefficient were obtained.

In order to visualize the flow in the region of the ice shape, a splitter plate arrangement was used. The plate could be inserted into place between the upper and lower halves of the simulated ice shape (Figure 10). Droplets of oil-based paint were applied and the tunnel brought from idle up to the required test speed. After no further movement of the droplets was observed, the tunnel was brought to idle and photographs were taken of the flow patterns(Figures 11-13). The separated streamline coordinates were digitized from these photographs for use in the mixed analysis/design study.

Five configurations were run during the two year program, including deflecting the flap from 0-30 degrees. Of importance to this report were results obtained on:

1). Glaze 3

2). Glaze 7

3). Generic Glaze

The Cp distributions and integrated lift coefficients provided the necessary database for the analysis effort which will be discussed in Chapter 5.

V. RESULTS AND DISCUSSION

Two approaches to evaluating the performance of a glaze ice shape were used in this study. Both relied upon the database generated in the Lewis Icing Tunnel on the simulated ice shapes. The first scheme was to examine current airfoil analysis codes and compare the predicted inviscid pressure distribution to the experimental result. The second approach utilized the Bristow inviscid design and analysis program in an attempt to predict the shape of the separated zone behind the glaze ice horn. Together with this effort equivalent body concepts were investigated.

Analysis of Current Potential Flow Schemes

As a first attempt at analyzing glaze ice accretions, an investigation of current airfoil analysis programs was performed. Computer programs utilized in this phase were Smetana, Eppler, Dvorak, Bristow, and Theodorsen.

To initially evaluate these programs, sample cases were run on the clean 63A415 airfoil and compared to experimental results obtained in the Lewis Icing Tunnel. A representative comparison is shown in Figure 14. This particular distribution is at $\alpha=2.6^{\circ}$ and was obtained from the Bristow code, but the results of all the programs studied were nearly identical. Good agreement with experiment was seen.

An interesting observation can be made about the various panelling methods described in Chapter 3 of this text. Throughout this phase of the study, very little difference was seen among the pressure distributions generated by the Eppler and Bristow programs. However, Cp distributions from the Eppler analysis do show a higher degree of sensitivity to the coordinates. This can be seen in the higher frequency and magnitude of pressure spikes, particularly in the leading edge region. This is primarily due to the means by which Eppler cubic splines the input coordinates to define the panels. Smoothing of all ice shapes was a necessity for input to this program.

The first ice shape to be examined, the Glaze 7 case, was a logical progression from the clean airfoil. As seen from Figure 6, this shape is monotonically increasing in X. Figure 15 shows a resulting pressure distribution from the comparisons made. Prediction again is very good at this angle of attack, 4.6°. However, as the angle of attack was increased and the laminar separation bubble in the region of the ice shape horns grew, the potential flow results were not very good. This is understandable in light of the highly viscous nature of the separation bubble.

Three of the studied computer programs had boundary layer routines; Dvorak, Eppler, and Smetana. However none had the capability to predict the separation bubble geometry and flow properties. When laminar separation was predicted, the bubble was assumed to be small enough to be considered negligible. Thus re-attachment was predicted at the same location as separation. The flow was then considered turbulent from this point on. However, due to the large adverse gradient in this area the turbulent boundary layer routines soon predict separation also. It should be noted that the laminar separation point predicted by Dvorak compared very well with the observed flow visualization separation point.

Flow visualization techniques however reveal the true size of the separation bubble (Figures 11-13). Bubble lengths of 10% chord were observed at moderate angles of attack. This definitely shows that the assumptions made by these computer programs, even though valid for most cases, break down when applied to the flow in the region of the ice growth.

The Glaze 3 and Generic Glaze shapes, due to the fact that they are not monotonically increasing in X, proved to be much more difficult to analyze. The Smetana program simply would not run on a double-valued shape and the Theodorsen conformal mapping method (Figure 16) could not successfully map the iced airfoil to the circle plane.

Another difficulty arose at this time with the Dvorak program. Figures 17-19 show the panel geometry produced by the Bristow, Dvorak, and Eppler codes respectively, for the Glaze 3 case. While Bristow and Eppler modelled the large change in slope very well (Bristow does not redistribute the coordinates) , Dvorak's method poorly approximated the geometry. Figure 18 shows a panelling attempt by Dvorak for the Glaze 3 shape. The lower horn was not retained in the panelled configuration. This inability to correctly represent the input geometry was seen throughout the analysis of the Glaze 3 and Generic Glaze shapes.

Figures 20-22 show the comparisons between theory and experiment for the Glaze 3 ice shape at a low angle of attack. Reasonable accuracy is obtained for this case. However, when the angle of attack was increased, results degraded quickly. Figures 23-25 show the Generic Glaze shape at a moderate angle of attack, 5.6°. As the angle of attack of the airfoil with ice is increased, the viscous effects become quickly much more important than for clean airfoils at a similar angle.

Figure 23 shows the difficulty associated with trying to treat a viscous flow problem with an inviscid approach. The large pressure spike, observed with all ice shapes, occurs at the tip of the horn as the flow attempts to negotiate the large change in surface slope at this point. None of the programs examined could predict the observed constant pressure zone associated with the laminar separation bubble.

Even though comparisons between theory and experiment made at low angles of attack were good, when moderate angles are evaluated the viscous effects associated with the ice shape need to be considered. Table 2 shows this very clearly. It should be noted that the theory row corresponds to an averaging of the results from Bristow, Dvorak, and Eppler for that angle of attack (Smetana was included for the Glaze 7 cases). Figure 26 shows a summary of the characteristics of the airfoil analysis methods investigated. The next step in the analysis then was to examine the shape and length of the laminar bubble.

TABLE 2

Lift Coefficient Prediction with Ice

GLAZE 3

α	-2.4	3.6	5.6	9.6

Theory	0.10	0.84	1.09	1.57
Experiment	0.08	0.75	1.01	1.18

GLAZE 7

α	-3.4	2.6	4.6	8.6
Theory	-0.03	0.72	0.96	1.45
Experiment	-0.03	0.70	0.90	1.30

GENERIC GLAZE

α	-2.4	-0.4	1.6	3.6	5.6
Theory	0.10	0.35	0.60	0.85	1.10
Experiment	0.10	0.32	0.54	0.72	0.84

Mixed Analysis/Design Method

The Bristow program has the unique option of performing mixed analysis and design problems. This feature was utilized in an effort to predict the shape of the laminar separation zone.

The input to the Bristow mixed analysis/design option involved holding the geometry fixed at the tips of the ice horn (1 panel was fixed on each horn). In addition, tangential and normal velocities in the design region were required. All normal velocity components were set to zero. The tangential component was then calculated from the experimental pressure coefficients and Bernoulli's Equation.

Since quantitative flow visualization data was only available for comparison for the upper surface, the geometry of the bubble in this region was studied primarily. However, conclusions drawn here should apply in the lower surface separated zone and the region between the two ice horns. From the photographs of the splitter plate arrangement (Figures 11-13), digitized coordinates for these regions were obtained for comparison to theory.

One final parameter needed to be examined before prediction of the bubble geometry could be made. This parameter, the reattachment point, is the position on the airfoil up to which velocities are specified and beyond which geometry is fixed. Figure 27 shows the predicted geometry of a separation bubble on the Glaze 3 shape. The reattachment point was varied from X=.04 to X=.80 . The shape of the bubble converged to the solid line in this figure. Moving this point further back on the airfoil surface did not alter the shape of the bubble. Therefore, for the cases examined here rear position of the design region was set to X=.20 .

Figure 28 shows a comparison between predicted and experimental shapes of the separation bubble. Reasonable agreement is seen at this low angle of attack. However, as the angle of attack was increased, the predicted shape tended to be longer and thicker than the observed one. Figure 29 shows a comparison run on the Glaze 3 shape at 5.6°. Experimentally, the reattachment point was observed to be at X=.05 . Theoretically however, it was found to be at X=.175 .

There are a number of reasons for these discrepancies. First, with a splitter plate technique of this kind, the line that is visualized is actually a little above the zero velocity line (Figure 3), not the separated streamline. This would agree with the observation that the splitter plate shape lies within the bounds of the theoretical prediction.

A second, and far more important difficulty was discovered while studying the flow visualization photographs. In Figure 11, the streamlines are observed to converge, indicative of a flow no longer 2-D in nature. A test program was performed in the OSU Subsonic Wind Tunnel to determine the nature of this problem [21].

A GAW-1 airfoil was outfitted with a splitter plate and a simulated glaze ice shape. The airfoil was run through a series of angles of attack, first with the splitter plate leading edge protruding out into the stream, and second with this portion of the plate removed. The results of this study show that with the larger splitter plate, the boundary layer separates off the plate and induces vortices due to the impressed adverse pressure gradient from the ice shape. These vortices traveled downstream, affecting the 2-D nature of the flow near the splitter plate. Quantitative measurements showed a change in re-attachment point of 5% was possible between the two plates. This value however cannot be directly applied to the results on the 63A415 airfoil in the IRT. Rather, the reader should use this information qualitatively when applying it to Figures 28-29. The important point is that the large splitter plate moved the reattachment point forward on the airfoil surface. Keeping this factor in mind the prediction of the separated zone in Figures 28 and 29 appear to be better than first thought.

A third difficulty with this type of mixed-mode analysis and design comes from the assumption that the pressure gradient through the boundary layer is negligible. This assumption is a key element of the design process but may not be a valid one for the thick separation zones associated with glaze ice.

Lastly, comparison with flow visualization is not possible in the region between the glaze horns due to the reasons just mentioned. However, Figure 30 shows the predicted geometry using this method for the Glaze 3 shape at $\alpha=5.6^{\circ}$.

Equivalent Body Approach

The last phase of this study looked at the equivalent body approach in which pressures were calculated on the input observed separated streamline. Figures 31-33 show the pressure distribution in the separated zone for the Glaze 3 airfoil at $\alpha=5.6^{\circ}$. Respectively these results are from the Bristow, Dvorak, and Eppler codes. The dashed lines represent an inviscid solution obtained from the physical airfoil geometry only. The solid lines are the improvement obtained when the coordinates of the separated streamline from the flow visualization are input. The improvement does not appear very significant for this case but that is primarily due to the position and extent of the bubble. It should be noted that the coordinates of the separated streamline were not smoothed before input. As a result, a large pressure gradient is obtained where the separated streamline rejoins the airfoil surface (Figure 29).

Figures 34-35 show another comparison with a thicker and longer separation bubble. With this case, a vast improvement is obtained between the inviscid prediction based on the actual geometry and that based on the separated streamline. Particular notice should be taken of the comparison in the area of the separated zone behind the ice shape horn. Lastly, a test was performed of the design method of the Bristow code using these conditions. The pressure distribution calculated by Bristow for the separated streamline, Figure 34, was re-input as a design region. The geometry predicted from this distribution is shown in Figure 36 along with the original separated streamline geometry. Excellent agreement is obtained and substantiates the use of the Bristow program for these applications.

VI. SUMMARY AND CONCLUSIONS

An experimental program was conducted to expand the current database of performance data on airfoils with glaze ice. Simulated ice shapes were developed based on actual ice growth on the NACA 63A415 airfoil in the NASA Lewis Icing Research Tunnel. These shapes were tapped so pressure distributions could be obtained. In addition, flow visualization photographs were taken of a splitter plate arrangement in the region around the ice shape.

Extensive comparisons were run using current airfoil analysis programs such as Eppler and Smetana in an effort to predict the pressure distribution and separation zone geometry of these ice shapes. Also, comparisons were made using the Bristow Mixed Analysis/Design Program between the separated streamline geometry obtained from the flow visualization and the predicted geometry designed from input values of velocity. The following conclusions can be made from the study described here:

1. Most panelling methods can predict the pressure distribution of an airfoil with ice, but only at a low angle of attack. When the angle is increased to

moderate levels, the method breaks down because of the large separation bubble created and its viscous nature.

2. Panelling methods that do have boundary layer routines treat the laminar bubble as a transition point from laminar to turbulent flow. This transition is considered to occur in a negligible distance.

3. The classical assumption that the pressure gradient through the boundary layer is negligible appears to hold even for the thick separation zones associated with glaze ice accretions. Reasonable predictions of the bubble length and shape were obtained from this assumption.

4. Improved results are obtained from the theory when an equivalent body approach is applied. The coordinates of the separated streamline are input rather than the physical geometry of the airfoil surface.

It is recommended that before an attempt is made to develop a numerical approach to analyze glaze ice accretions, the following steps are taken:

1. Obtain more detailed pressure distributions in the

separated zone behind the ice horns and between them. The more detailed the surface pressure distribution is, the better the results the mixed analysis and design program yields.

2. Obtain pressures vertically through the separated zone. Also, at the same time measure the velocity profile in this region. Lastly, a determination should be made of the transition point from laminar to turbulent flow in the shear layer.

3. Repeat the splitter plate flow visualization experiments with a smaller plate so as not to ruin the 2-D nature of the flow. This will give a better idea where the reattachment point is.

USER'S GUIDE TO THE BRISTOW CODE

This chapter is intended as a user's guide for the Bristow program. Two modes of operation are possible with this program; 1) Analysis only and 2) Mixed Analysis and Design. Where applicable the differences in input parameters between these modes will be pointed out.

CARD 1 COLUMNS 1-72 ATITLE
Enter case title on this card.

CARD 2 COLUMNS 1-10 ISAVE
Set ISAVE=0 to indicate the start of a new set of geometry
Set ISAVE=2 for input of a new ALPHA only. Submit cards 1-2 only.
Set ISAVE=1 if only retaining QT and N(Q) from previous case. All other inputs can be changed. Untransformed (XB,YB) coordinates are reused.
Set ISAVE=3 to repeat last case with new values of ALPHA, CIRCE, and VNP distribution. No design cases are allowed. Only submit cards 1, 2, 6, 8, and 11.
COLUMNS 11-20 ALPHA
Angle of attack of x-axis with respect to free stream velocity

CARD 3 COLUMNS 1-10 QT
Number of airfoil elements (Normally set QT=1. If flap present set QT=2, etc.)

CARD 4 COLUMNS 1-10 CHORD
Reference length for moment and lift coefficient integration (Normally set=1)
COLUMNS 11-20 CAPPA1
Recommend set CAPPA1=.01 . Used in calculation of sharp corner control point
COLUMNS 21-30 CAPPA2
Recommend set CAPPA2=.02 . Used in calculation of

Kutta condition control points
COLUMNS 31-40 LINSIG
Singularity choices:
Set LINSIG=0 for constant source distribution on panels.
Set LINSIG=1 for VINF portion of source distribution to be piecewise constant and VNP portion to be piecewise linear.
Set LINSIG=2 for linear source distribution on panels
(NOTE: LINSIG Choice has little effect on results.
Recommend set LINSIG=0 or 2.
COLUMNS 41-50 VINF
Non-dimensional free stream velocity (Normally set=1)
COLUMNS 51-60 VREF
Non-dimensional reference velocity used to calculate pressure coefficients (Normally VREF=VINF)

CARD 5 COLUMNS 1-10 ITMAX
Number of iterations in design mode (Set=0 in analysis mode). Suggest set=4 for design mode. Most cases converge in this number of iterations.
COLUMNS 11-20 ITR
COLUMNS 21-30 RLX
Recommend set RLX=1.0 . Design region geometry is relaxed by a factor of RLX every ITR iterations.
COLUMNS 31-40 ITHICK
Normally set=0. Allows no thickness increase if design process results in negative thickness. Execution will terminate if this occurs. Set=1 and thickness increase will be allowed inspite of negative thickness occurring.

The following cards should be input for each of the

elements (Q=1, Q=2, ..., Q=QT)

CARD 6 COLUMNS 1-10 N
Number of coordinates defining element Q
COLUMNS 11-20 PT
Number of boundary conditions in element Q (PT = Number of analysis regions + number of design regions)
COLUMNS 21-30 KUTTA
Normally set=5. Set=1 to input desired circulation normalized by perimeter of this element. Set=2 to input circulation (not normalized by perimeter). Set=3 if Kutta condition is zero velocity normal to trailing edge bisector. Set=4 to determine

circulation from input tangential velocities. Set=5 for same condition as 3 but higher order extrapolation for trailing edge bisector is used (4 panels - 2 upper surface, 2 lower surface)
COLUMNS 31-40 CIRCP
Input circulation of this element. Set=0 for KUTTA>2
COLUMNS 41-50 DXTE
COLUMNS 51-60 DYTE
Trailing edge opening. Ignored if trailing edge regions are PTYPE=0 ($DXTE = X_N - X_1$) ($DYTE = Y_N - Y_1$)

CARD 7 COLUMNS 1-10 AQ
COLUMNS 11-20 BQ
COLUMNS 21-30 ALFQ
COLUMNS 31-40 SCLQ
Normally set AQ=0, BQ=0, ALFQ=1, and SCLQ=1. These are transformation parameters which are applied to input coordinates (XB,YB) to produce a new series of coordinates for use in the program. This allows translation, rotation, and stretching of the input coordinates. The transformation applied is:
X=AQ+SCLQ*[XB*COS(ALFQ)-YB*SIN(ALFQ)]
Y=BQ+SCLQ*[YB*COS(ALFQ)+XB*SIN(ALFQ)]
COLUMNS 41-50 ICLK
Set=0 for internal flow (counter-clockwise coordinate input). Set=1 for external flow (clockwise coordinate input).

The following cards are input for each of the regions P=1, P=2, ..., P=PT of element Q.

CARD 8 COLUMNS 1-10 NPAN
Number of panels in this boundary condition region (NOTE: NPAN=N-1)
COLUMNS 11-20 ISHP
Set=0 if first point in the region is not a sharp corner point
Set=1 if first point in the region is a sharp corner point (NOTE: a sharp corner point is defined as a point of slope discontinuity)
COLUMNS 21-30 PTYPE
Set=0 if analysis region with no translation
Set=1 if analysis region with translation allowed
Set=2 if design region with first coordinate fixed and previous boundary condition was a design region

Set=3 if design region with first coordinate free or previous boundary condition region was analysis with no translation
COLUMNS 31-40 PDSF
Normally set=0. Set=1 for this region to undergo same relative length change as previous region. (NOTE:This region must be PTYPE=3 and previous region must be PTYPE$\geq$2)
COLUMNS 41-50 IVNP
Set=0 if normal velocities are prescribed in this region
Set=1 if normal velocities are all to be set to zero. This is normally the case.
COLUMNS 51-60 W
Normally set=.001. If large number is input length variation is suppressed.

CARD 9 COLUMNS 1-10 XP
COLUMNS 11-20 YP
Coordinates of first point in this boundary condition region. Ignored if PTYPE$\neq$2.
COLUMNS 21-30 XBB
COLUMNS 31-40 YBB
If this is a design region and is followed by an analysis region, these coordinates are considered to be the last point in this region.

CARD 10 COLUMNS 1-10 VNP of Panel 1
⋮
COLUMNS 51-60 VNP of Panel NPAN
Omit this card if IVNP=1. Otherwise enter panel midpoint normal velocities.
COLUMNS 61-70 NRD
Number of values of VNP on this card. Omit if 6 values of VNP are on this card or it is the last card for this region.

NEXT CARD SERIES
COLUMNS 1-10 VTP of Panel 1
⋮
COLUMNS 51-60 VTP of Panel NPAN
Omit this card if analysis region. Otherwise enter panel midpoint tangential velocities.
COLUMNS 61-70 NRD
Same as NRD of card 10.

NEXT CARD SERIES
COLUMNS 1-10 VTPP of Panel 1
⋮
COLUMNS 51-60 VTPP of Panel NPAN

Omit this card if analysis region. Otherwise enter panel endpoint tangential velocities.
CCLUMNS 61-70 NBD
Same as NBD of card 10

Input the next series of cards for element Q=1, Q=2, ..., Q=QT. Omit these cards if ISAVE=0.

NEXT CARD SERIES
CCLUMNS 1-10 XB of point 1 on this element
. .
. .
CCLUMNS 51-60 XB of point N on this element
X-coordinates of airfoil geometry. If external flow, input should be clockwise. If internal flow input is counter-clockwise.
CCLUMNS 61-70 NBD
Same as NBD of card 10

NEXT CARD SERIES
CCLUMNS 1-10 YB of point 1 on this element
. .
. .
CCLUMNS 51-60 YB of point N on this element
Y-coordinates of airfoil geometry. If external flow, input should be clockwise. If internal flow input is counter-clockwise.
CCLUMNS 61-70 NBD
Same as NBD of card 10

LIST OF REFERENCES

1) Editors of Flying Magazine, Pilot Error, New York: Van Nostrand Reinhold Company, 1977

2) Bragg, M.B. and Gregorek, G.M., "Predicting Aircraft Performance Degradation Due to Ice Accretion", SAE Technical Paper Series 830742, presented at the SAE Business Aircraft Meeting and Exposition, Wichita, Kansas, April 12-15, 1983

3) Bragg, M.B. and Gregorek, G.M., "Wind Tunnel Investigation of Airfoil Performance Degradation Due to Icing", AIAA Paper No. 82-0582, presented at the 12th Aerodynamic Testing Conference, Williamsburg, Virginia, March 22-24, 1982

4) Bragg, M.B., Zaguli, R.J., and Gregorek, G.M., "Wind Tunnel Evaluation of Airfoil Performance Using Simulated Ice Shapes", NASA CR 167960, November 1982

5) Gray, Vernon H., "Prediction of Aerodynamic Penalties Caused by Ice Formation on Various Airfoils", NASA TN D-2166, February 1964

6) Gray, Vernon H. and von Glahn, Uwe H., "Aerodynamic Effects Caused by Icing of an Unswept NACA 65A004 Airfoil", NACA TN 4155, 1957

7) "Aircraft Icing", AGARD Advisory Report No. 127, presented at AGARD Fluid Dynamics Panel Roundtable Discussion on Aircraft Icing, Ottawa, Canada, September 30, 1977

8) Dvorak, F.A. and Woodward, F.A., "A Viscous / Potential Flow Interaction Analysis Method for Multi-Element Infinite Swept Wings", NASA CR 2476, November 1974

9) Eppler, Richard and Somers, Dan M., "A Computer Program for the Design and Analysis of Low-Speed Airfoils", NASA TM 80210, August 1980

10) Venkateswarlu, K. and Marsden, D.J., "Prediction of Boundary Layer Developement in the Presence of a Laminar

Separation Bubble", Department of Mechanical Engineering, University of Alberta

11) Crimi, Peter and Reeves, Barry L., "Analysis of Leading Edge Separation Bubbles on Airfoils", AIAA Journal, Vol. 14, No. 11, December 1976

12) Ingelamn-Sundberg, M., Trunov, O.K., and Ivaniko, A., "Methods for Prediction of the Influence of Ice on Aircraft Flying Characteristics", a joint report from the Swedish-Soviet Working Group on Scientific-Technical Cooperation in the Field of Flight Safety, 6th Meeting, 1977

13) Shaw, Robert J. and Sotos, Ray G., "An Experimental Study of Airfoil Icing Characteristics", NASA TM 82790, January 1982

14) Pfeiffer, N.J. and Zumwalt, G.W., "A Computational Model for Low Speed Flows Past Airfoils with Spoilers", AIAA Paper No. 81-0253, presented at the 19th Aerospace Sciences Meeting, St. Louis, Missouri, January 12-15, 1981

15) McLachlan, B.G. and Karancheti, K., "Experimental Study of the Flowfield of an Airfoil with Deflected Spoiler", AIAA Paper No. 82-0126, presented at the 20th Aerospace Sciences Meeting, Orlando, Florida, January 11-14, 1982

16) Bristow, D.R. and Grose, G.G., "Modification of the Douglas Neumann Program to Improve the Efficiency of Predicting Component Interference and High Lift Characteristics", NASA CR 3020, August 1978

17) Smetana, Frederick O., Summey, Delbert C., Smith, Neill S. and Carden, Ronald K., "Light Aircraft Lift, Drag, and Moment Prediction- A Review and Analysis", NASA CR 2523, May 1975

18) Schlichting, H., Boundary Layer Theory, Sixth Edition, McGraw-Hill, New York, 1968

19) Zaguli, R.J., Bragg, M.B., and Gregorek, G.M., "Results of an Experimental Program Investigating the Effects of Simulated Ice on the Performance of the NACA 63A415 Airfoil with Flap", AARL TR 8301, May 1983

20) Freuler, R.J. and Hoffmann, M.J., "Experiences With An Airborne Digital Computer System for General Aviation Flight Testing", AIAA Paper No. 79- Paper No. 79-1834,

presented at the AIAA Aircraft Systems and Technology Meeting, New York, New York, August 20-22, 1979

21) Kunchal, David, "Splitter Plate Analysis", Final Report for AAE 693, Ohio State University, October 1982

22) Bristow, Dean R., "Multi-Element Airfoil Inviscid Analysis and Design Program (Version 1) User Instructions", McDonnell Aircraft Company, St. Louis, Missouri, December 1980

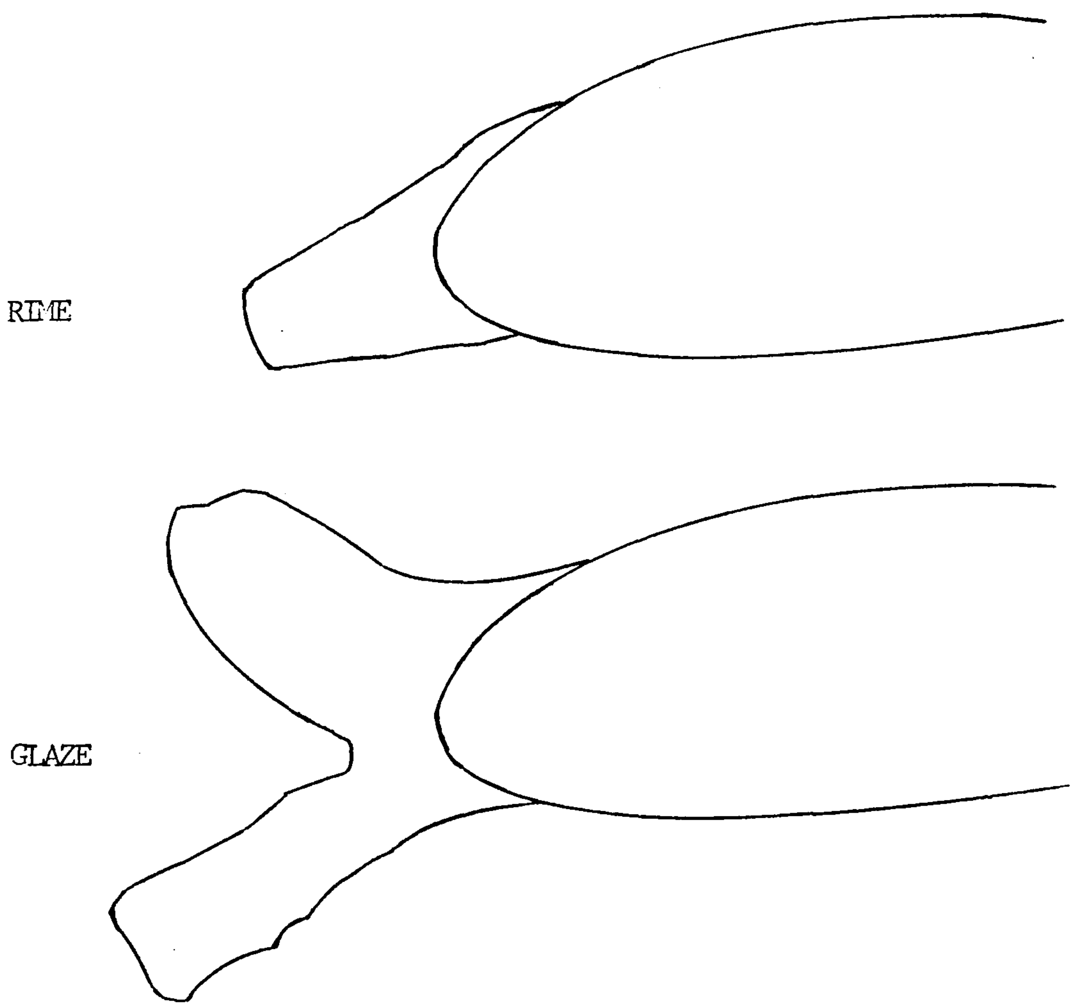

FIGURE 1. TYPICAL RIME AND GLAZE ICE ACCRETIONS ON AN AIRFOIL

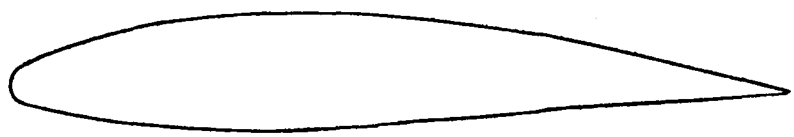

PHYSICAL AIRFOIL SHAPE

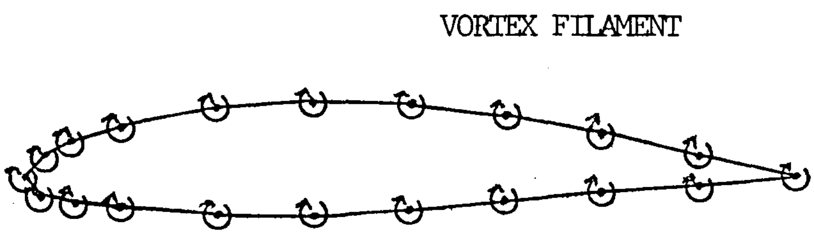

REPRESENTATION OF AIRFOIL BY POLYGON
AND POINT VORTICES

FIGURE 2. SMETANA PANELLING METHOD

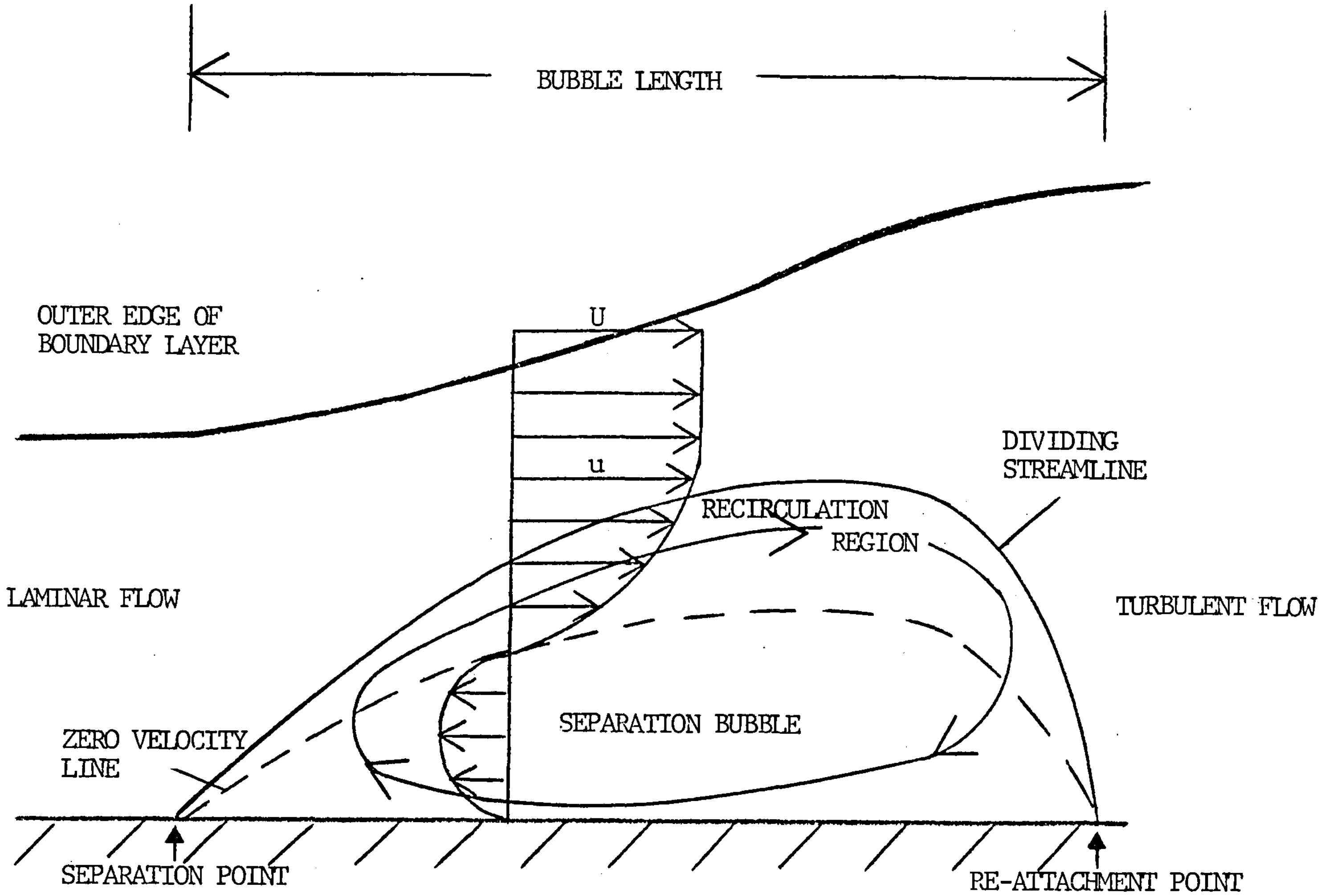

FIGURE 3. DIAGRAM OF LAMINAR SEPARATION BUBBLE

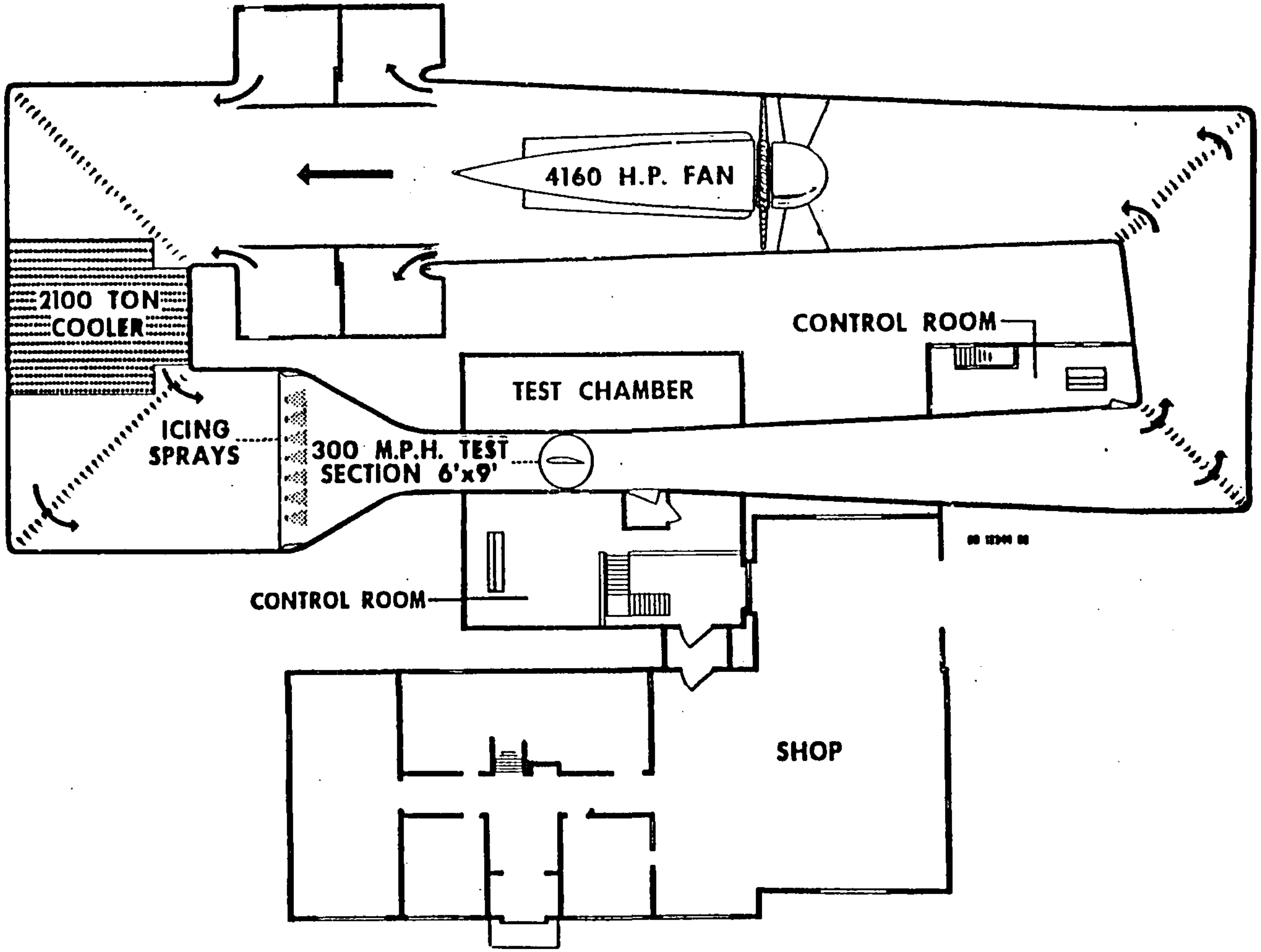

FIGURE 4. THE NASA LEWIS 6' x 9' ICING RESEARCH TUNNEL

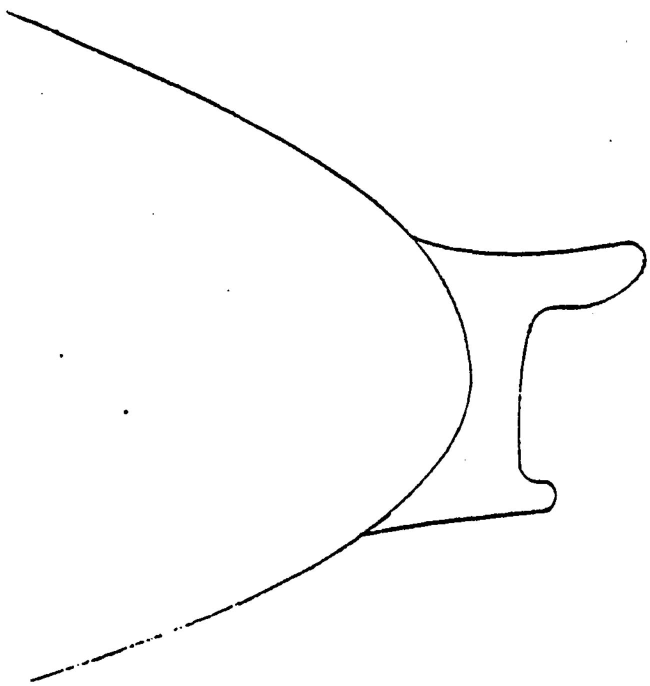

X/C	Z/C
-.00232	.01435
-.01019	.01389
-.01667	.01407
-.01944	.01315
-.01907	.01019
-.00648	.00241
-.00556	-.00593
-.00889	-.01204
-.00389	-.01389
.00667	-.01482

FIGURE 5. GLAZE 3 SIMULATED ICE ACCRETION AND PRESSURE TAP LOCATIONS

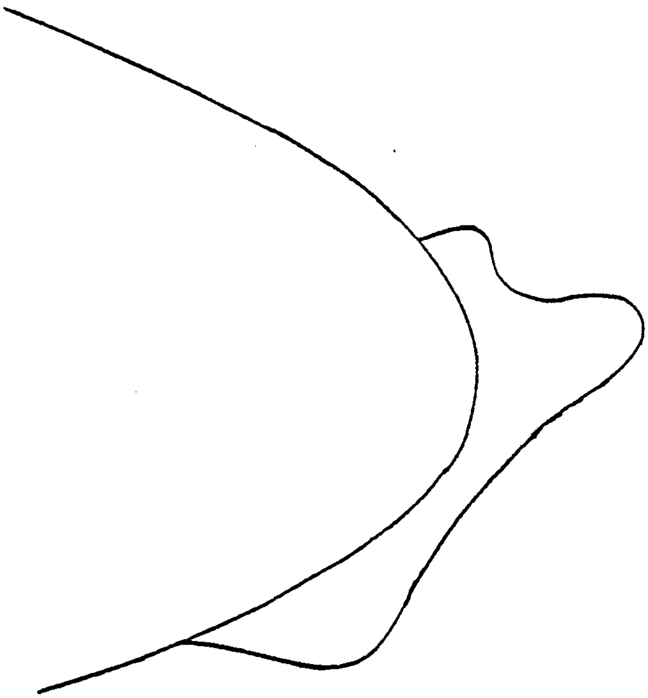

X/C	Z/C
.00093	.01759
-.00278	.01620
-.00648	.00972
-.01667	.00778
-.01796	.00519
-.01157	-.00093
-.00509	-.00602
.00556	-.01759
.01435	-.02732
.02500	-.02593

FIGURE 6. GLAZE 7 SIMULATED ICE ACCRETION
AND PRESSURE TAP LOCATIONS

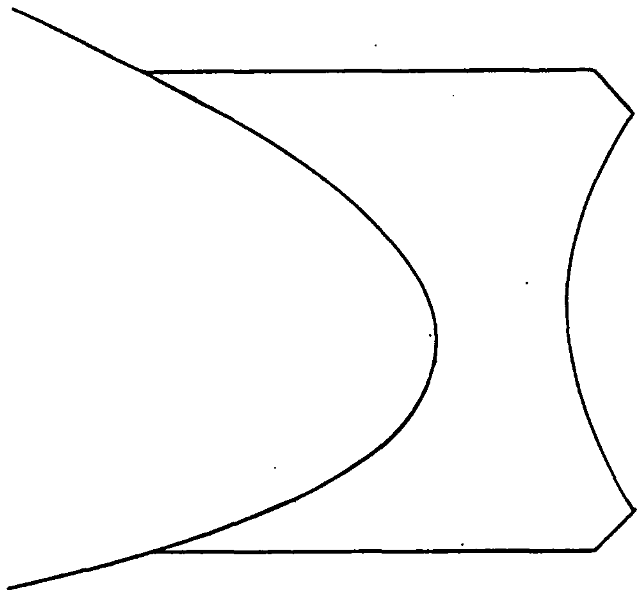

X/C	Z/C
0.01985	0.03807
0.00427	0.03807
- 0.01133	0.03807
- 0.02452	0.03584
- 0.02136	0.02264
- 0.01857	0.00706
- 0.02099	- 0.00854
- 0.02452	- 0.02229
- 0.00613	- 0.02414
0.01467	- 0.02414

FIGURE 7. GENERIC GLAZE SIMULATED ICE ACCRETION AND PRESSURE TAP LOCATIONS

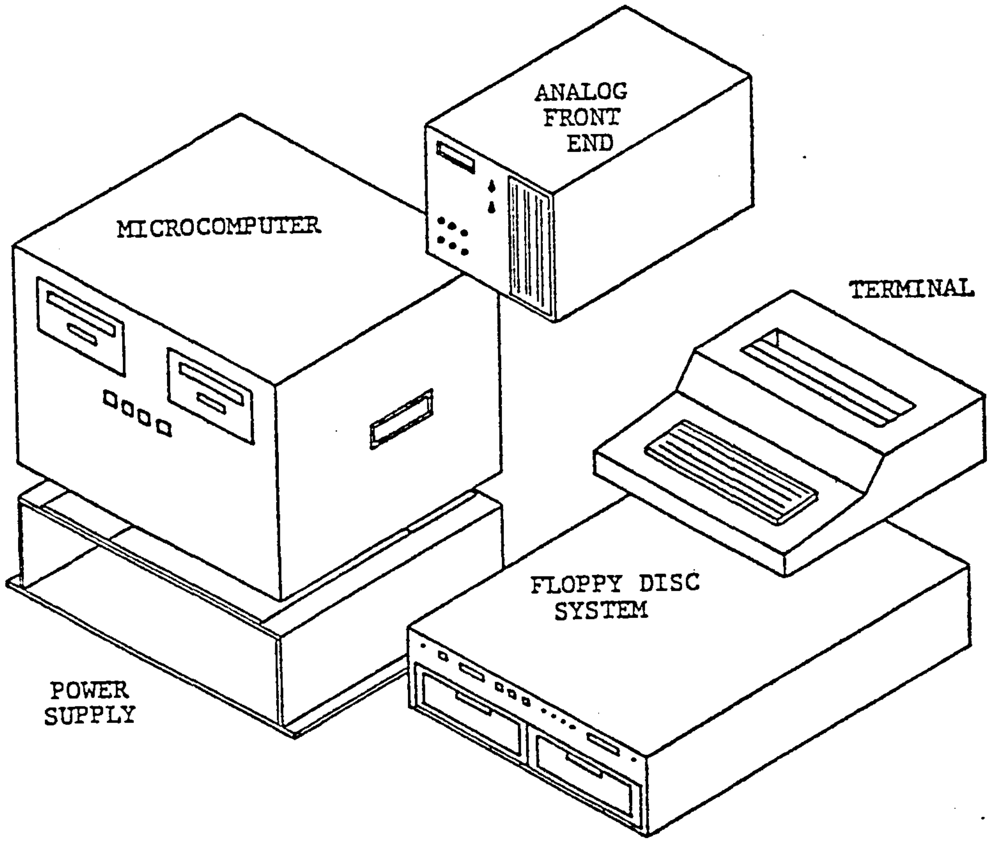

FIGURE 8. OSU DIGITAL DATA ACQUISITION AND REDUCTION SYSTEM

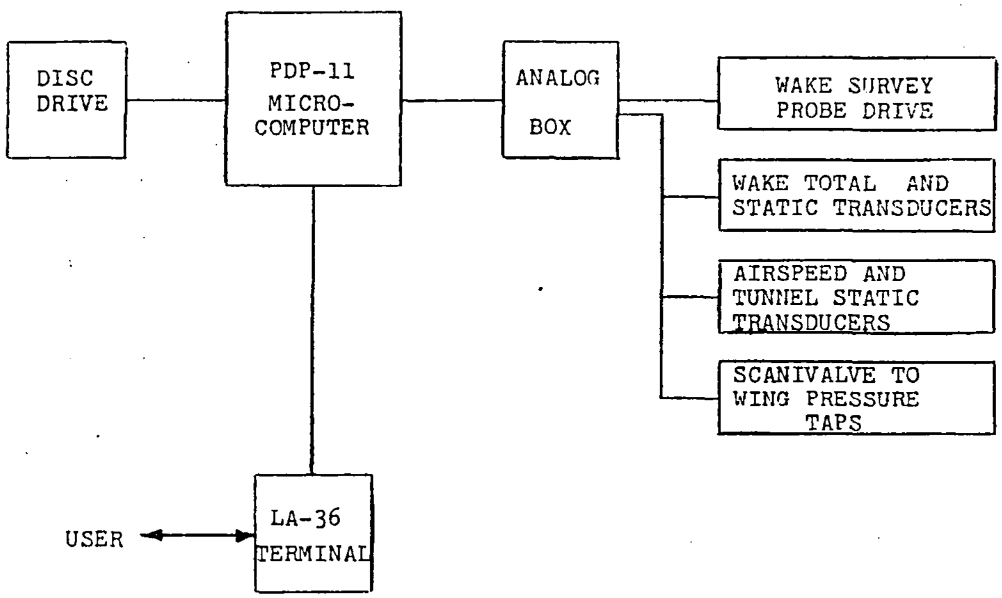

FIGURE 9. OSU DATA ACQUISITION SYSTEM
AS USED IN THE NASA LEWIS IRT

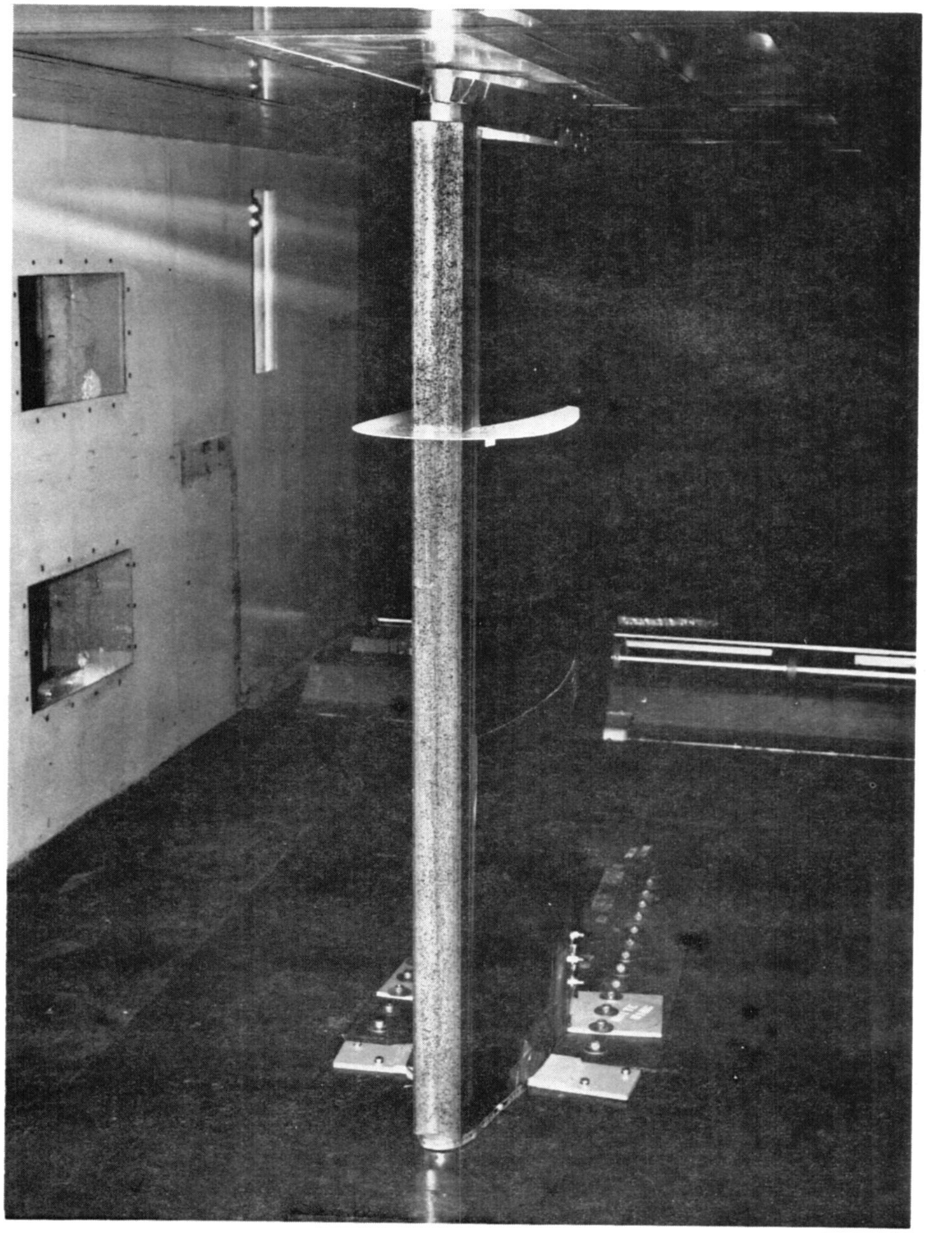

FIGURE 10. SPLITTER PLATE ON 63A415 AIRFOIL

Upper Surface
M = 0.152
Re = 4.7×10^6

FIGURE 11. SPLITTER PLATE PHOTOGRAPH OF GENERIC GLAZE ICE SHAPE ON 63A415 AIRFOIL (α=-0.4°)

Upper Surface
$M = 0.152$
$Re = 4.7 \times 10^6$

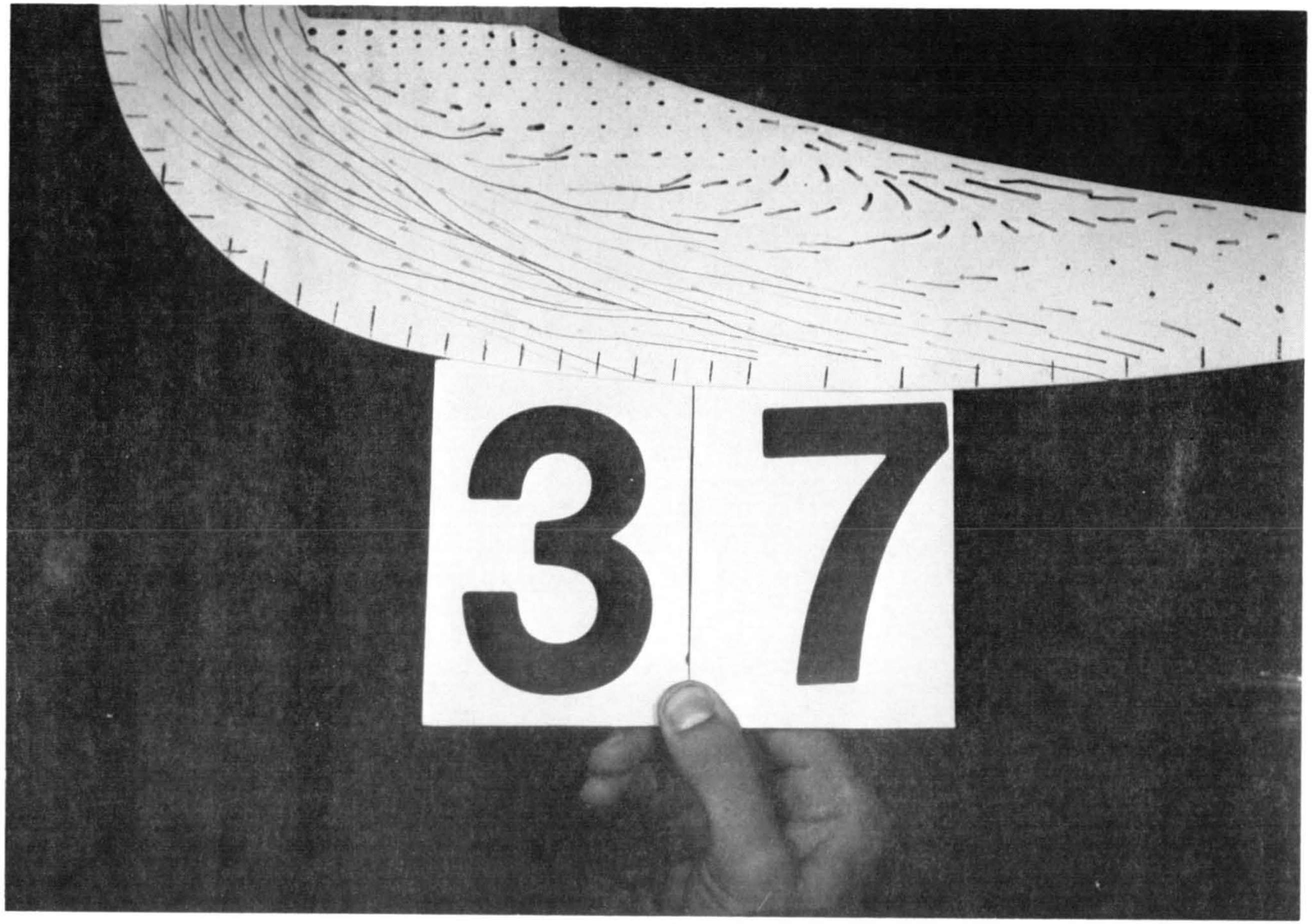

FIGURE 12. SPLITTER PLATE PHOTOGRAPH OF GENERIC GLAZE ICE SHAPE ON 63A415 AIRFOIL (α=5.6°)

Upper Surface
$M = 0.153$
$Re = 4.6 \times 10^6$

FIGURE 13. SPLITTER PLATE PHOTOGRAPH OF GLAZE 3 ICE SHAPE ON 63A415 AIRFOIL (α=5.6^{o})

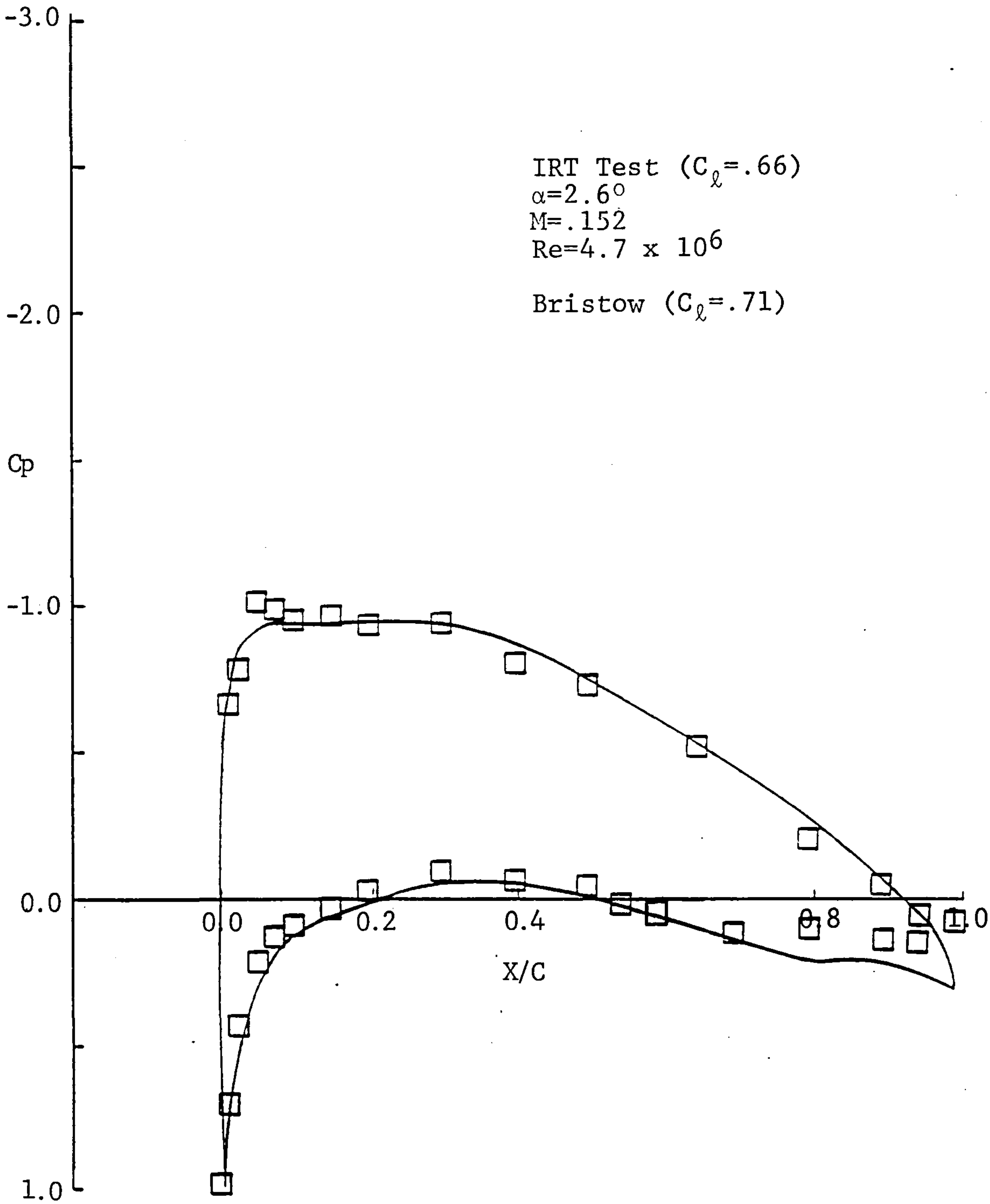

FIGURE 14. COMPARISON BETWEEN EXPERIMENT AND THEORY FOR THE 63A415 AIRFOIL

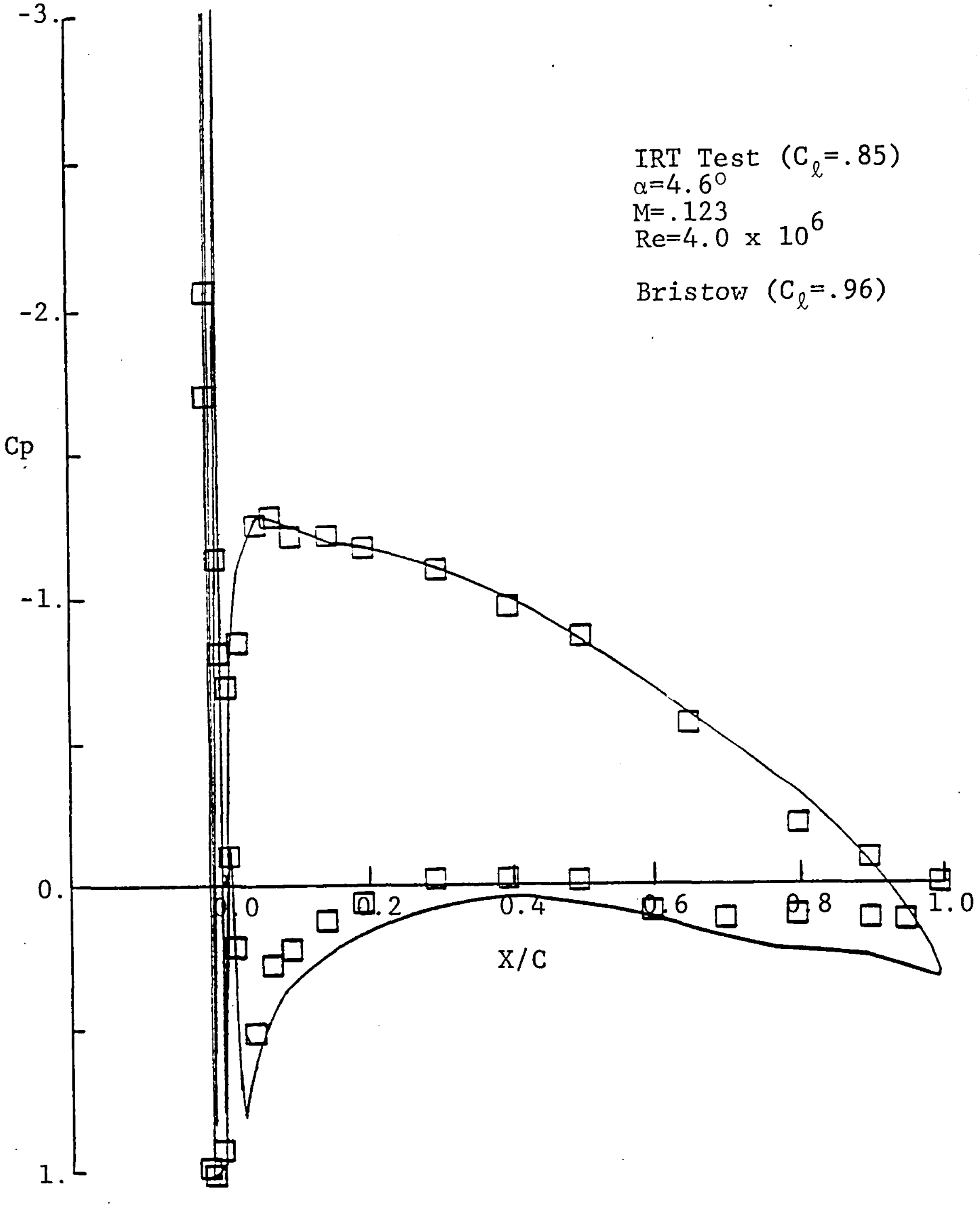

FIGURE 15. COMPARISON BETWEEN EXPERIMENT AND THEORY FOR THE 63A415 AIRFOIL WITH GLAZE 7 ICE SHAPE

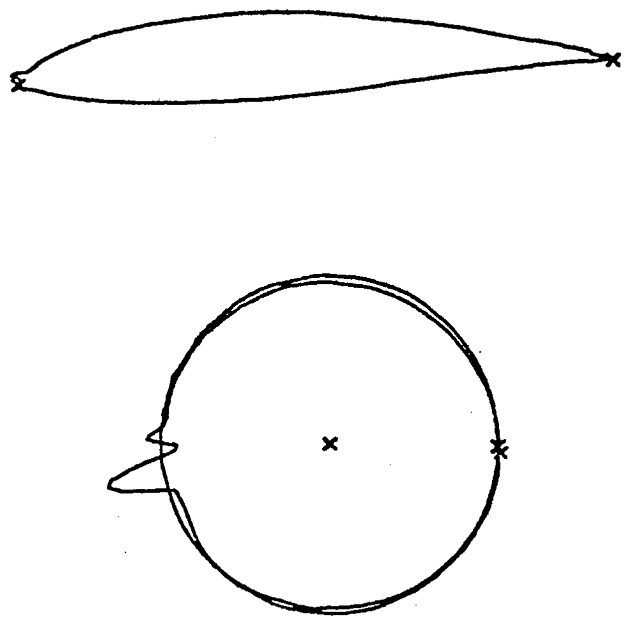

FIGURE 16. THEODORSEN TRANSFORMATION OF 63A415
AIRFOIL WITH GLAZE 3 ICE SHAPE

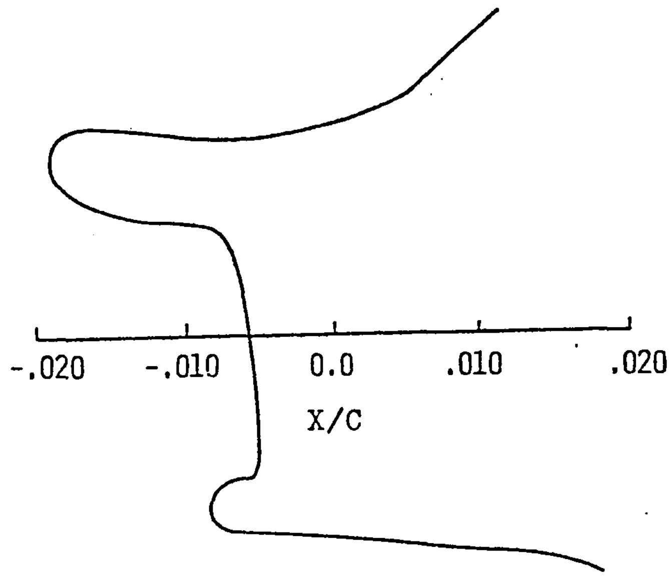

FIGURE 17. BRISTOW PANELLING SCHEME FOR GLAZE 3 ICE SHAPE

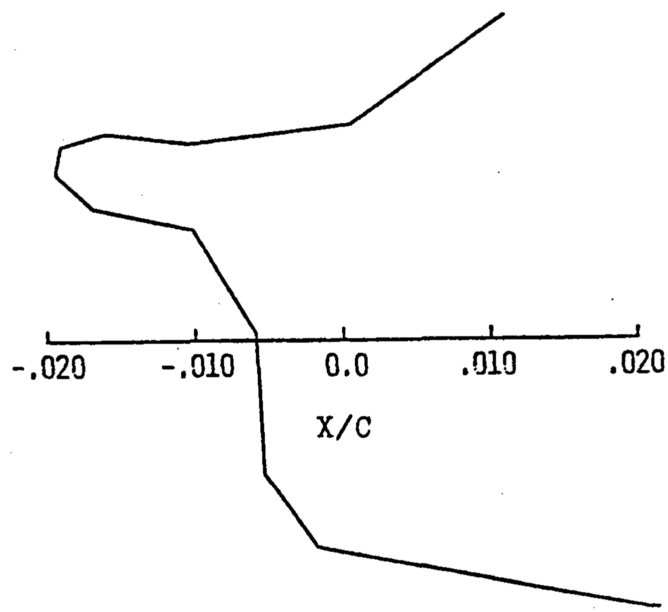

FIGURE 18. DVORAK PANELLING SCHEME FOR GLAZE 3 ICE SHAPE

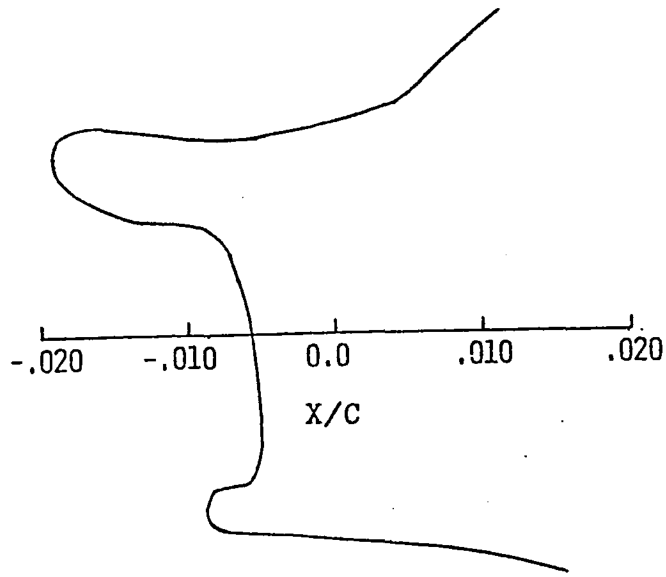

FIGURE 19. EPPLER PANELLING SCHEME FOR
GLAZE 3 ICE SHAPE

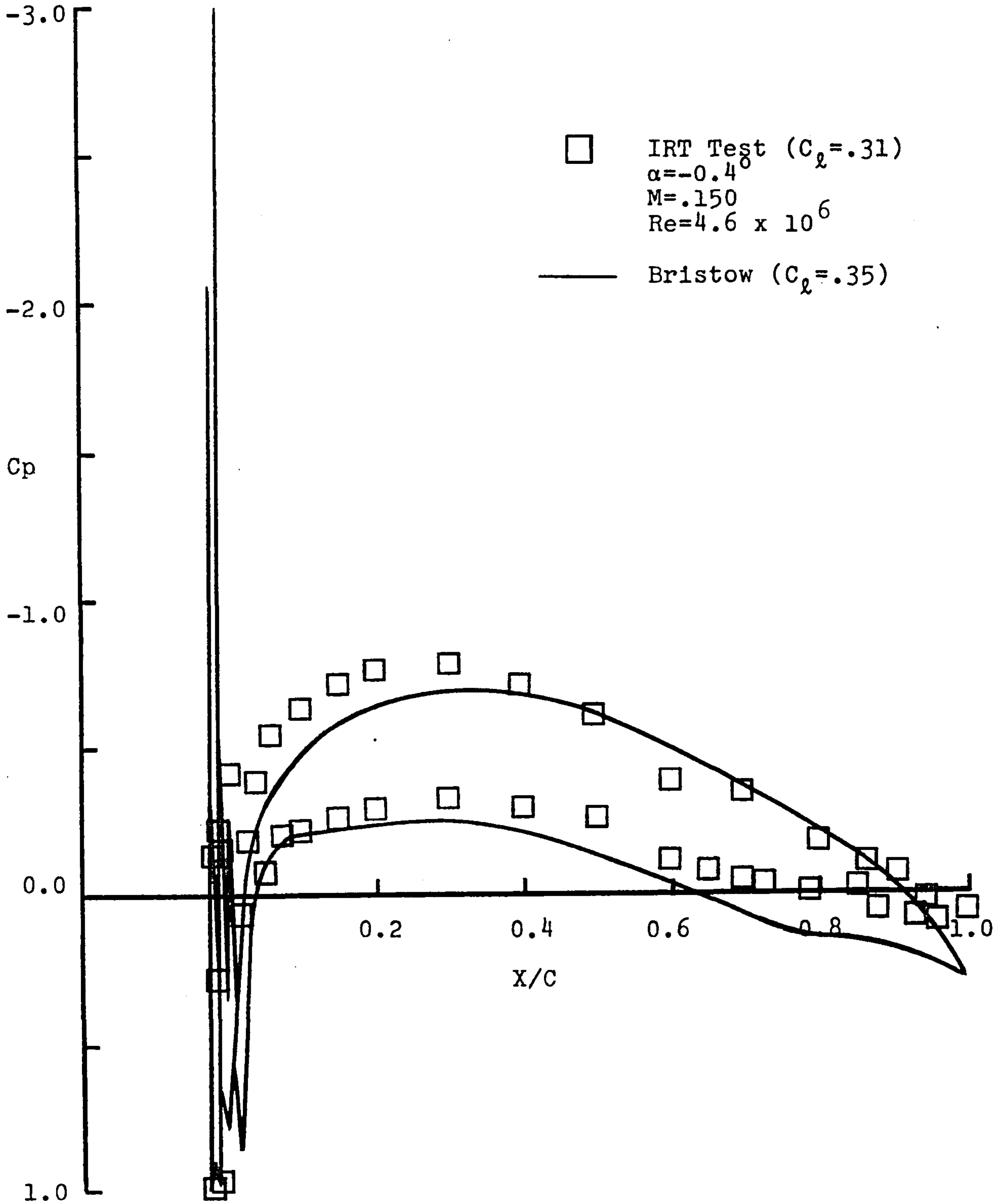

FIGURE 20. COMPARISON BETWEEN EXPERIMENT AND THEORY FOR THE 63A415 AIRFOIL WITH GLAZE 3 ICE SHAPE

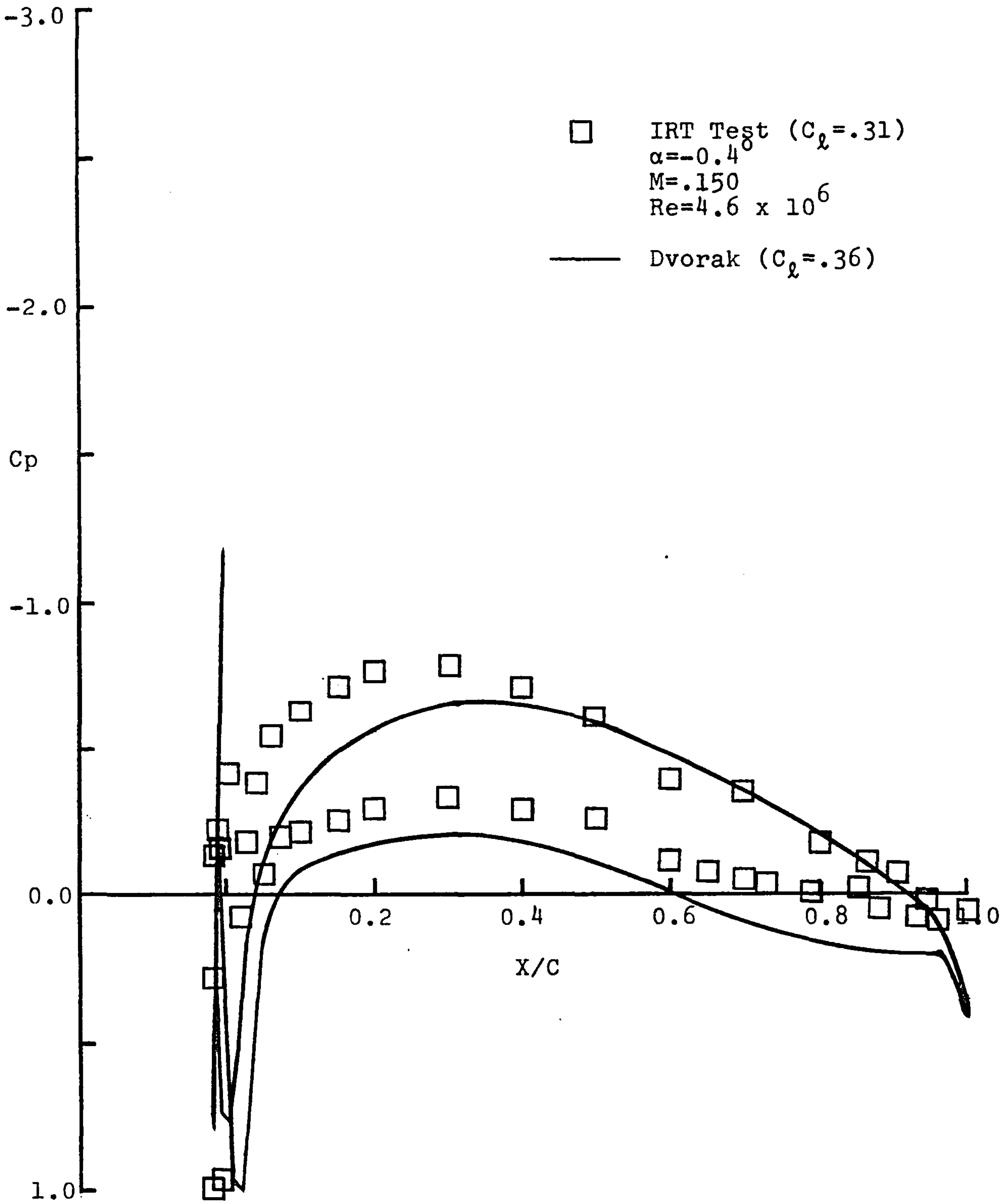

FIGURE 21. COMPARISON BETWEEN EXPERIMENT AND THEORY FOR THE 63A415 AIRFOIL WITH GLAZE 3 ICE SHAPE

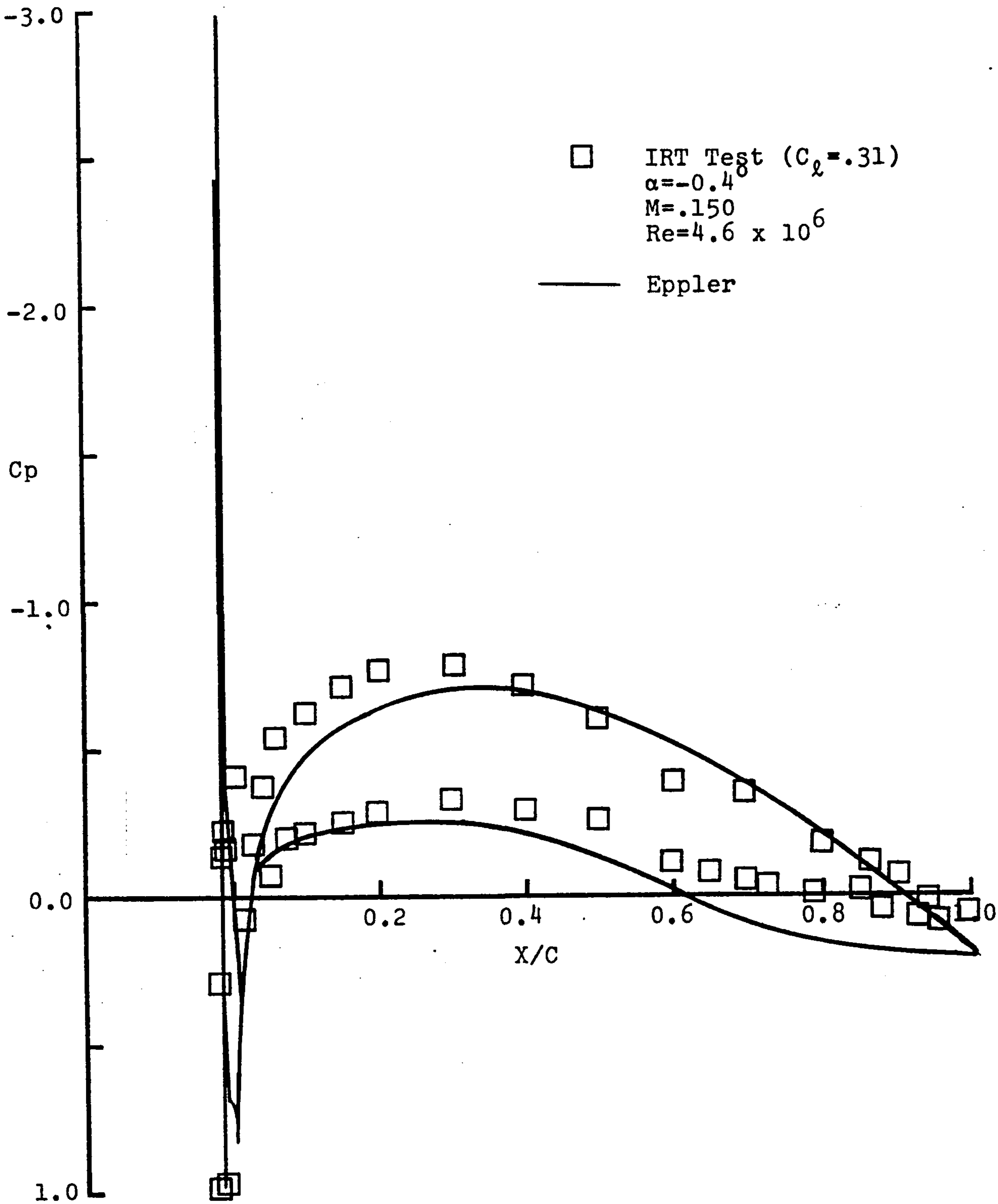

FIGURE 22. COMPARISON BETWEEN EXPERIMENT AND THEORY FOR THE 63A415 AIRFOIL WITH GLAZE 3 ICE SHAPE

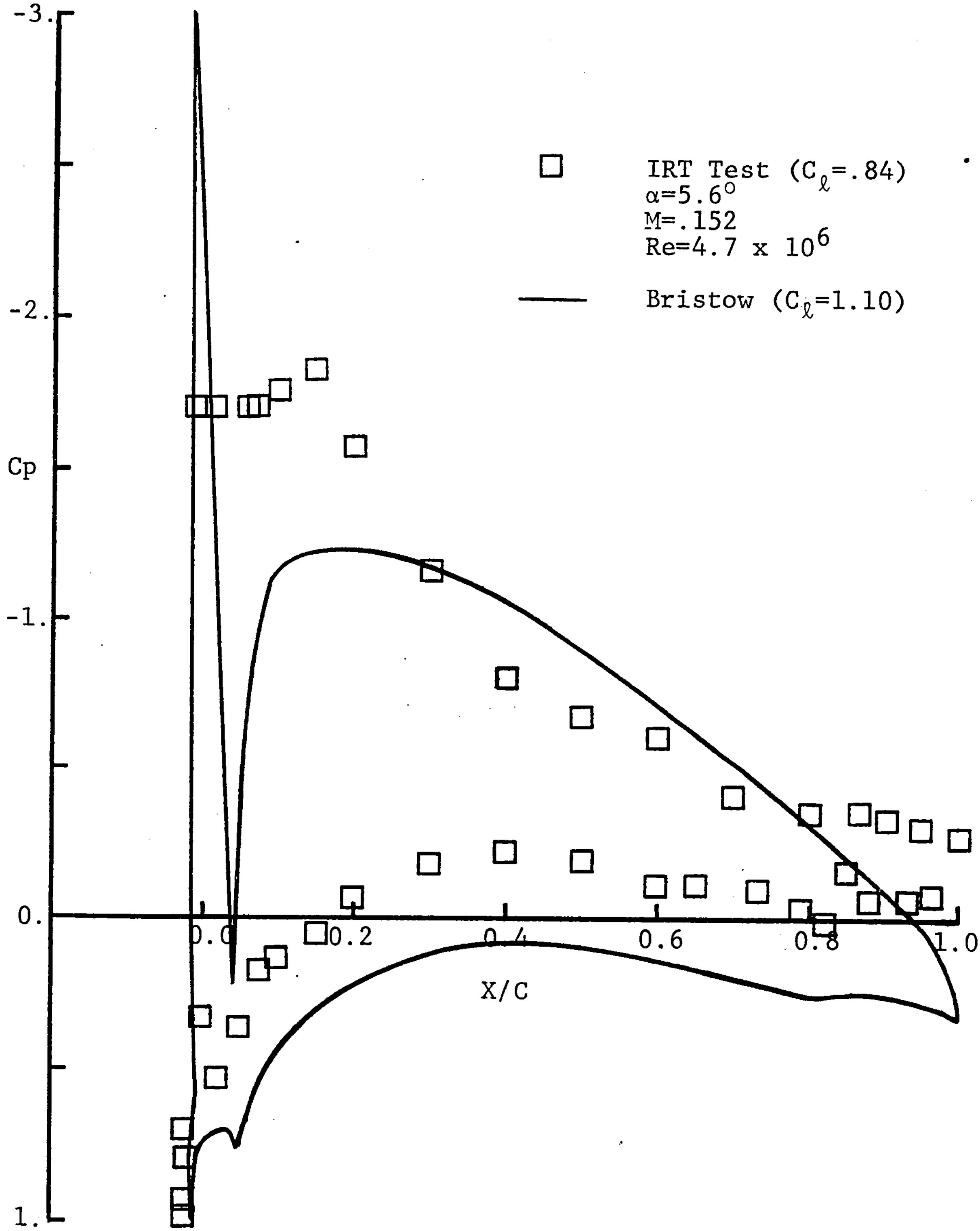

FIGURE 23. COMPARISON BETWEEN EXPERIMENT AND THEORY FOR THE 63A415 AIRFOIL WITH GENERIC GLAZE ICE SHAPE

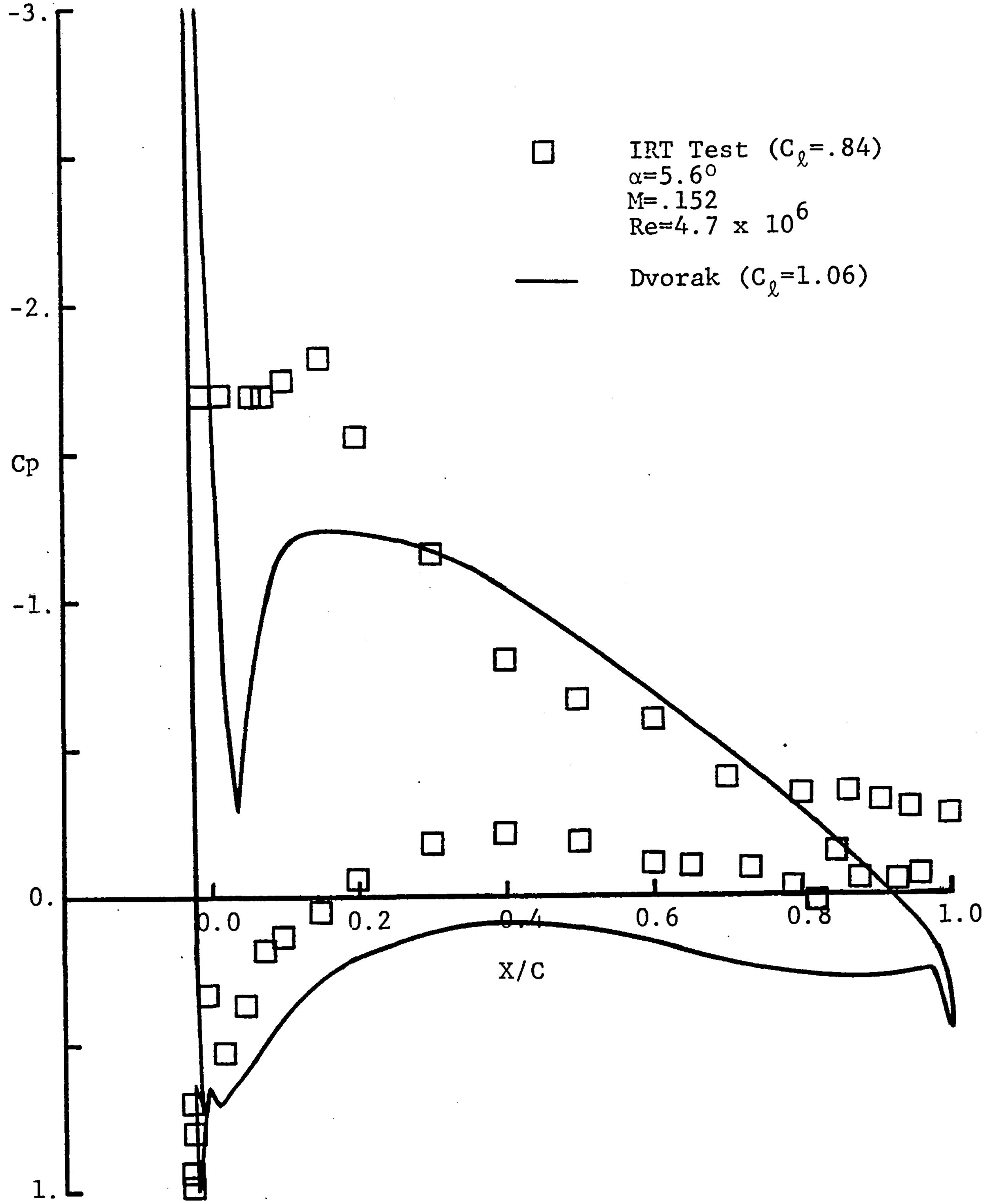

FIGURE 24. COMPARISON BETWEEN EXPERIMENT AND THEORY FOR THE 63A415 AIRFOIL WITH GENERIC GLAZE ICE SHAPE

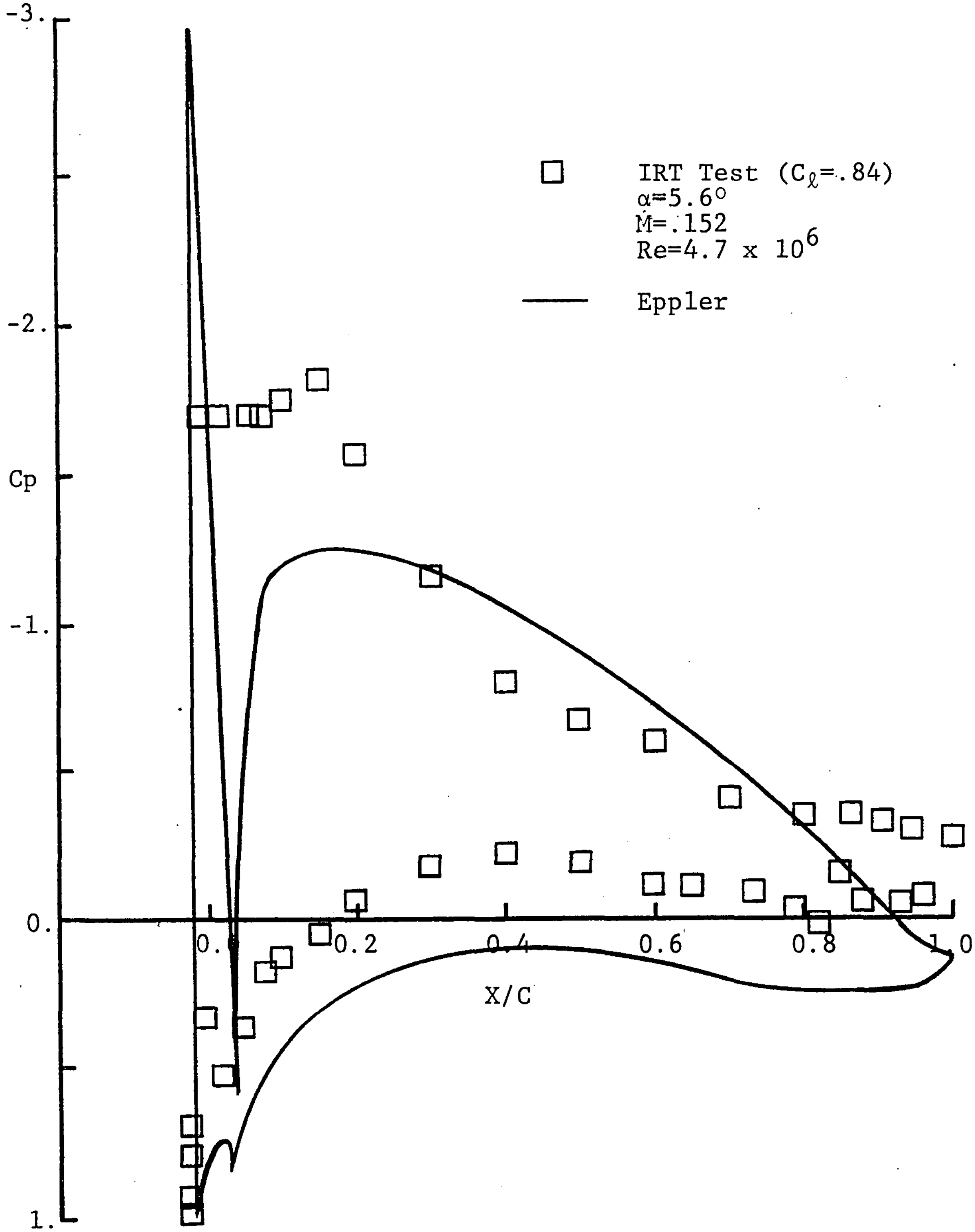

FIGURE 25. COMPARISON BETWEEN EXPERIMENT AND THEORY FOR THE 63A415 AIRFOIL WITH GENERIC GLAZE ICE SHAPE

CODE	POTENTIAL SOLUTION	RUN TIME	COMMENTS
EPPLER	MIXED PANEL METHOD PARABOLIC VORTICITY	2 MIN.	EXTREMELY SENSITIVE TO GEOMETRY REQUIRES ICE SHAPE SMOOTHING SPLINE FITS TO FORM PANELS, $C_{\ell_{MAX}}$ METHOD
SMETANA	PANEL METHOD CONSTANT VORTICITY	2 MIN.	X MONOTONICALLY INCREASING
DVORAK	PANEL METHOD LINEAR VORTICITY	2 MIN.	REDISTRIBUTES AIRFOIL COORDINATES POOR ICE SHAPE MODELLING $C_{\ell_{MAX}}$ METHOD
BRISTOW	PANEL METHOD SOURCE AND VORTICITY	5 MIN.	RELATIVELY INSENSITIVE TO ICE GEOMETRY MULTI-ELEMENT MODE DESIGN WITH MIXED BC
WOAN	THEODORSEN CONFORMAL MAPPING	1 MIN.	SENSITIVE TO GEOMETRY

FIGURE 26. FLOWFIELD PREDICTION METHODS SUMMARY

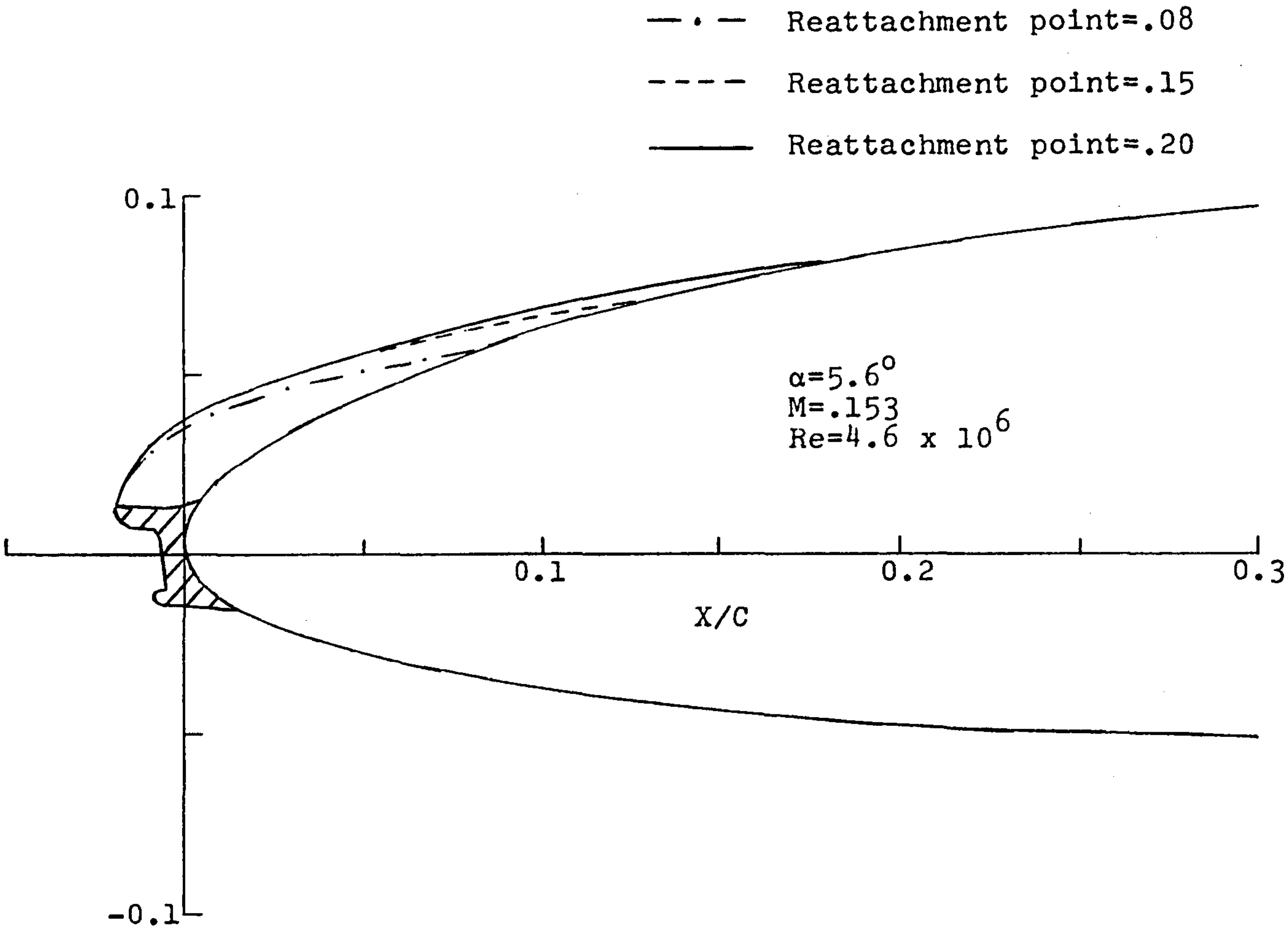

FIGURE 27. SEPARATION ZONE PREDICTION FROM MEASURED Cp's FOR THE 63A415 AIRFOIL WITH GLAZE 3 ICE SHAPE AND VARYING REATTACHMENT POINT

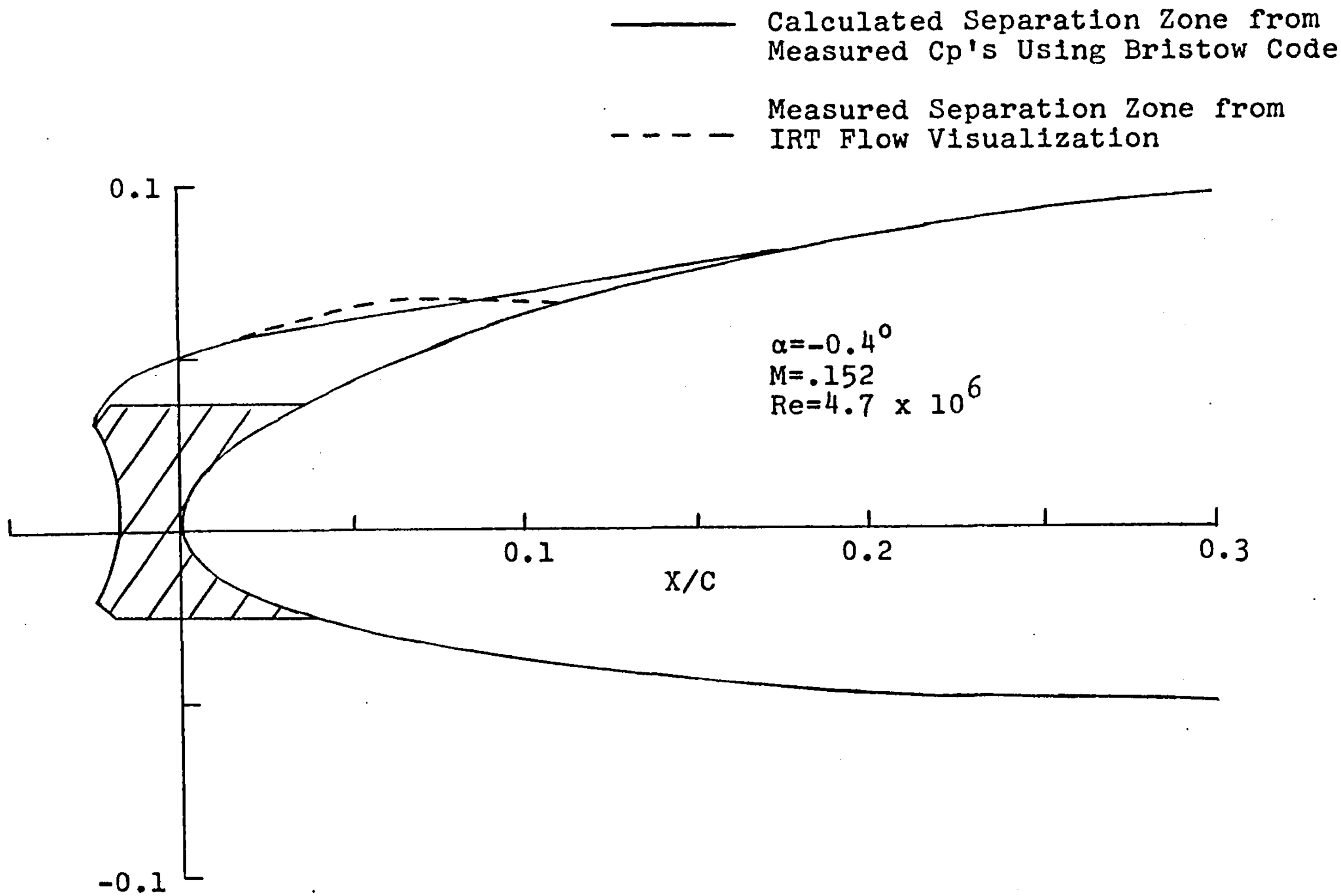

FIGURE 28. SEPARATION ZONE PREDICTION FROM MEASURED Cp's FOR THE 63A415 AIRFOIL WITH GENERIC GLAZE ICE SHAPE

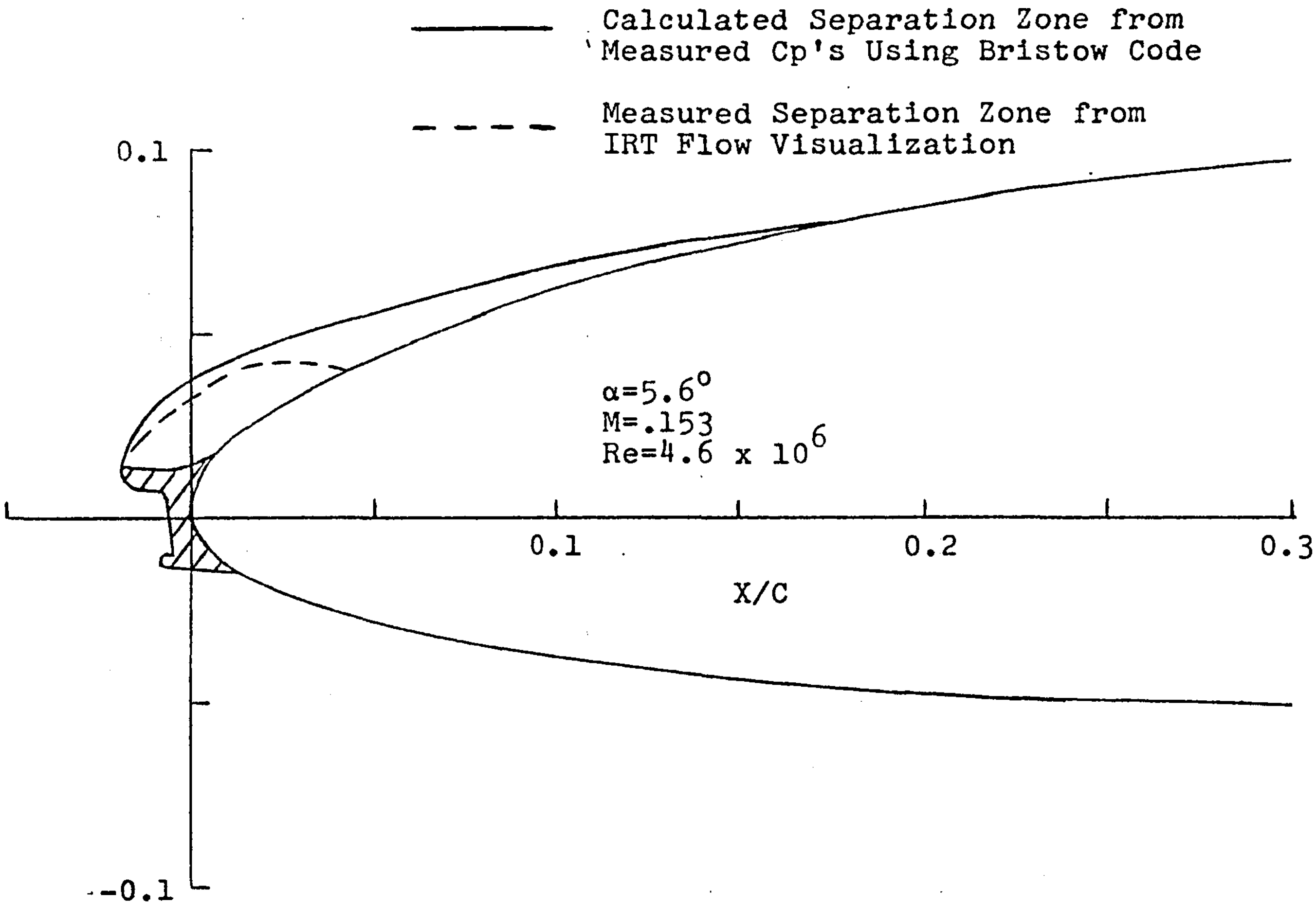

FIGURE 29. SEPARATION ZONE PREDICTION FROM MEASURED Cp's FOR THE 63A415 AIRFOIL WITH GLAZE 3 ICE SHAPE

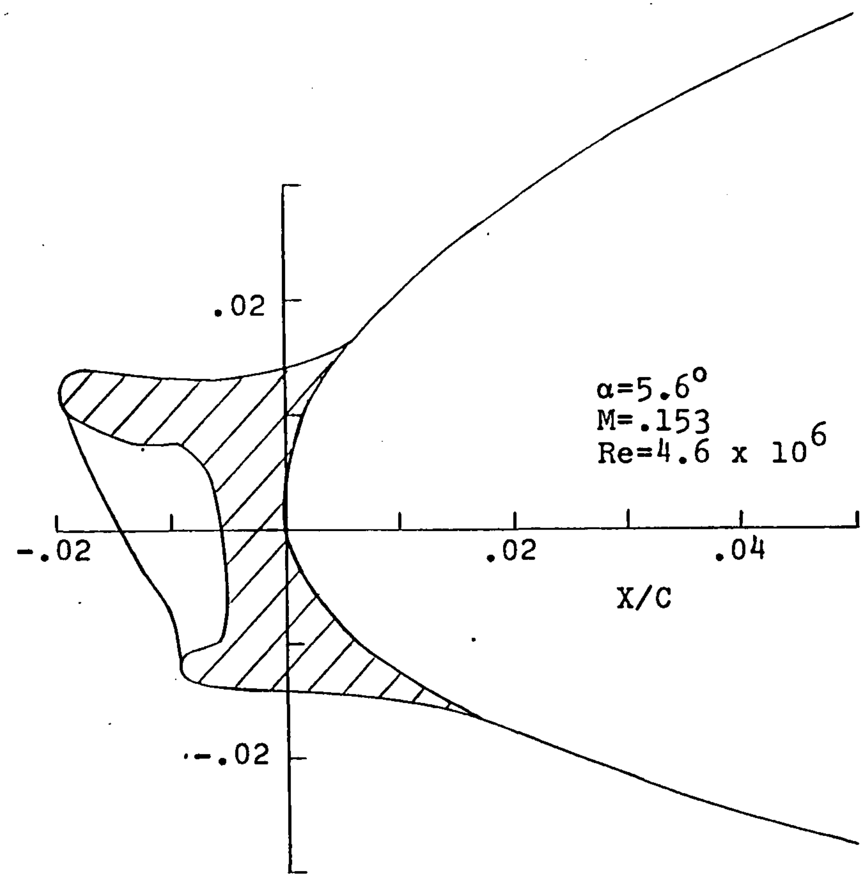

FIGURE 30. PREDICTION OF REGION BETWEEN GLAZE ICE HORNS FROM MEASURED Cp's FOR THE 63A415 AIRFOIL WITH GLAZE 3 ICE SHAPE

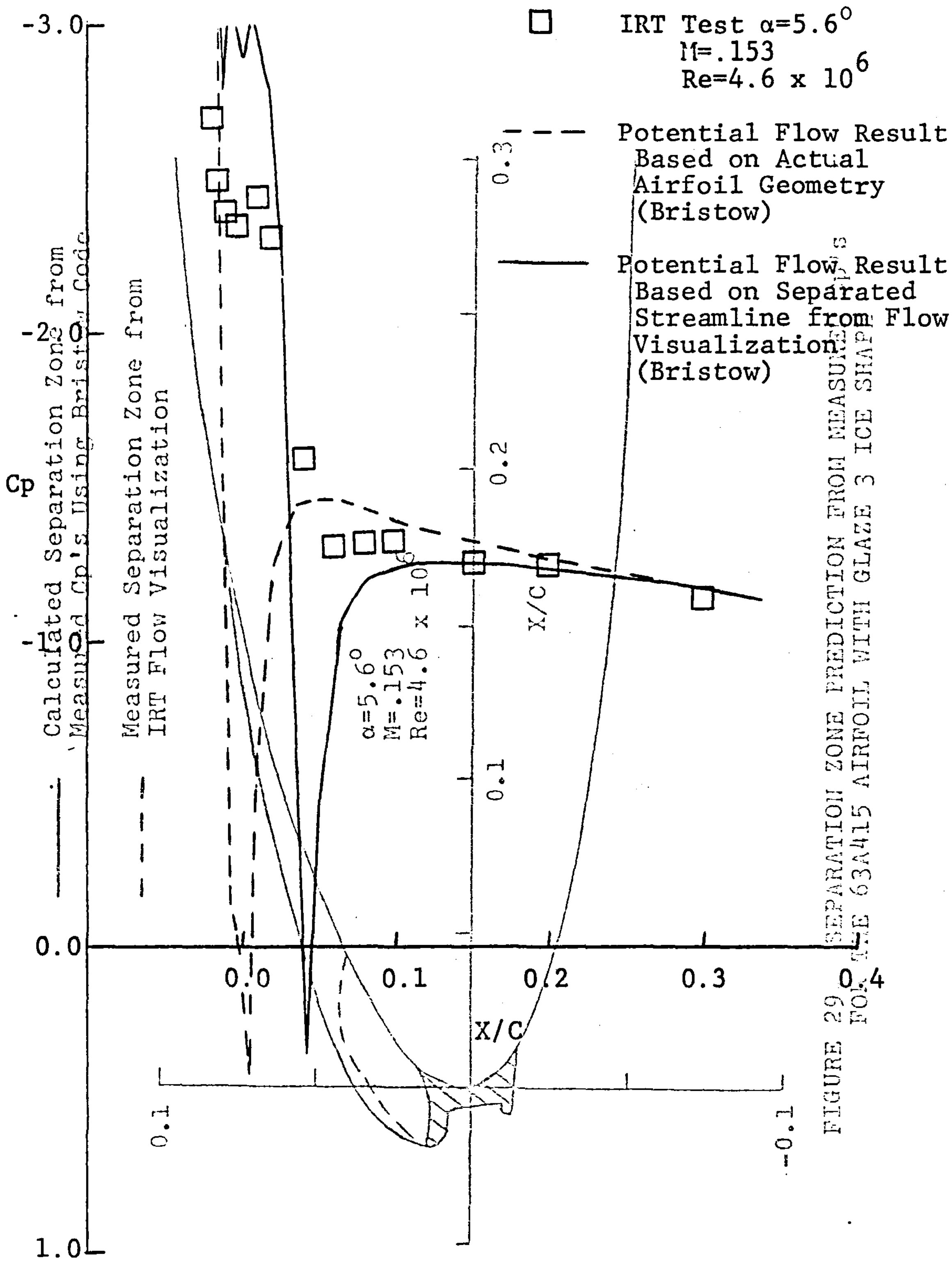

FIGURE 31. PRESSURE DISTRIBUTION IN SEPARATED ZONE BEHIND UPPER SURFACE HORN OF GLAZE 3 ICE SHAPE

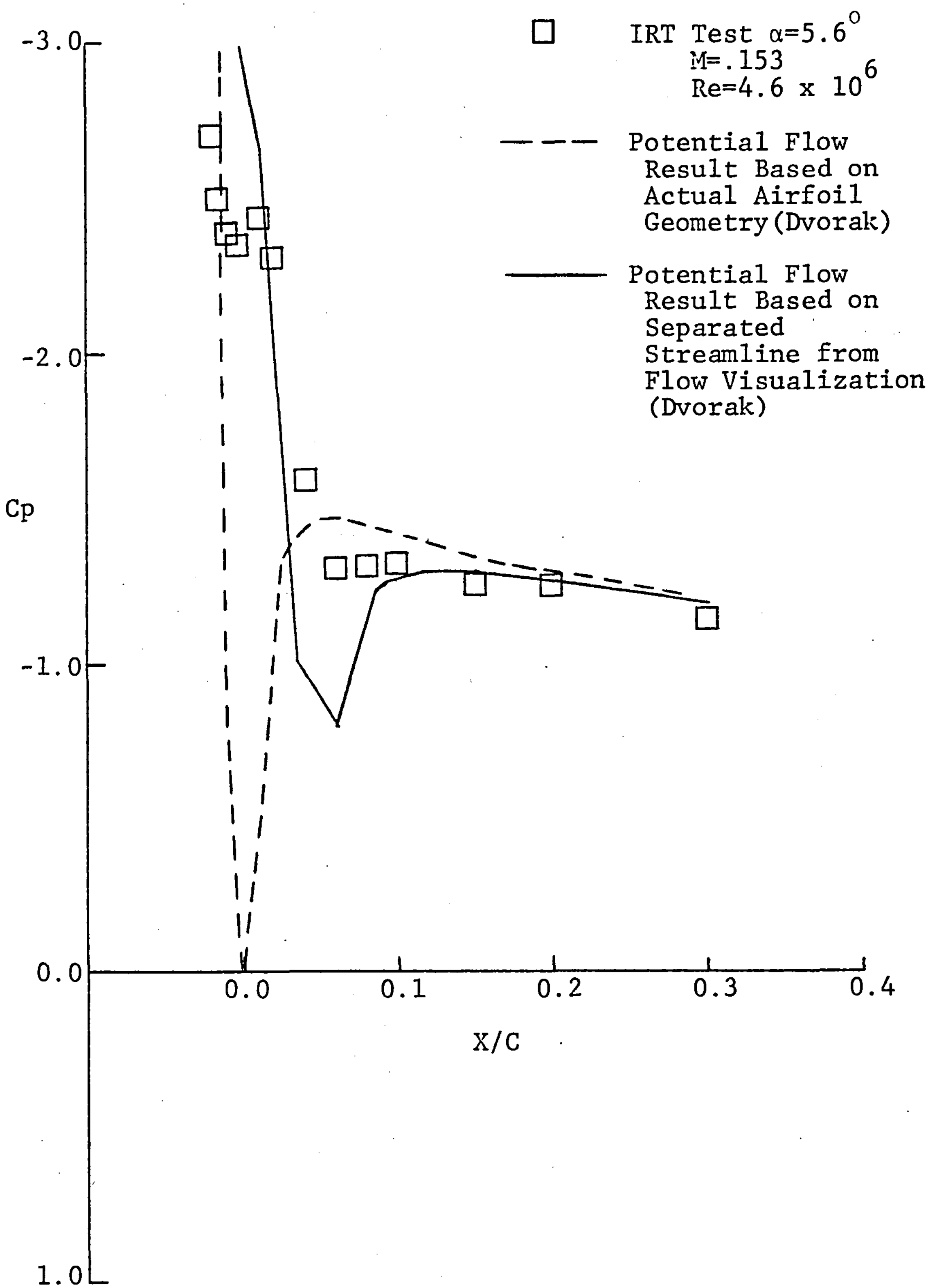

FIGURE 32. PRESSURE DISTRIBUTION IN SEPARATED ZONE BEHIND UPPER SURFACE HORN OF GLAZE 3 ICE SHAPE

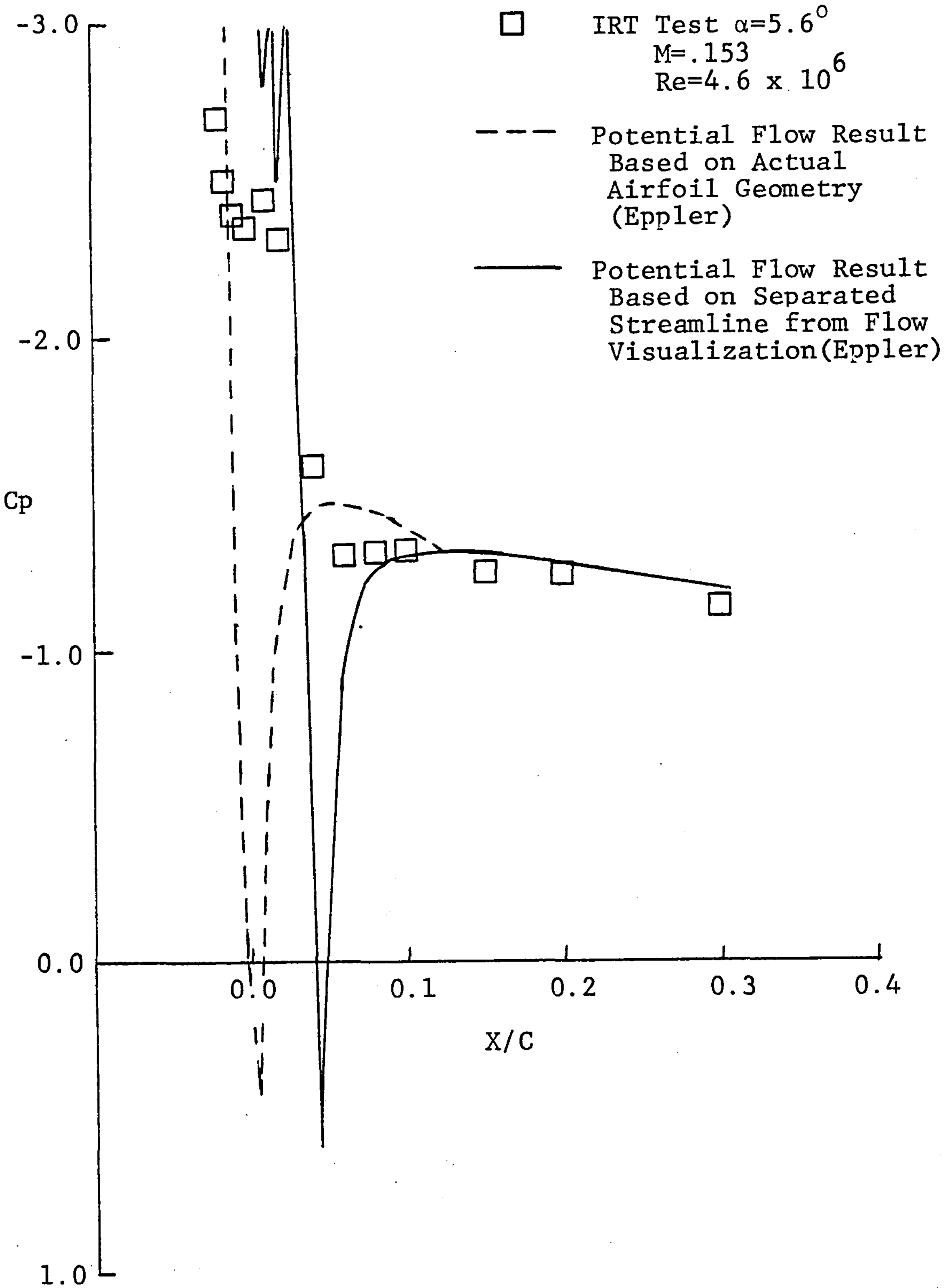

FIGURE 33. PRESSURE DISTRIBUTION IN SEPARATED ZONE BEHIND UPPER SURFACE HORN OF GLAZE 3 ICE SHAPE

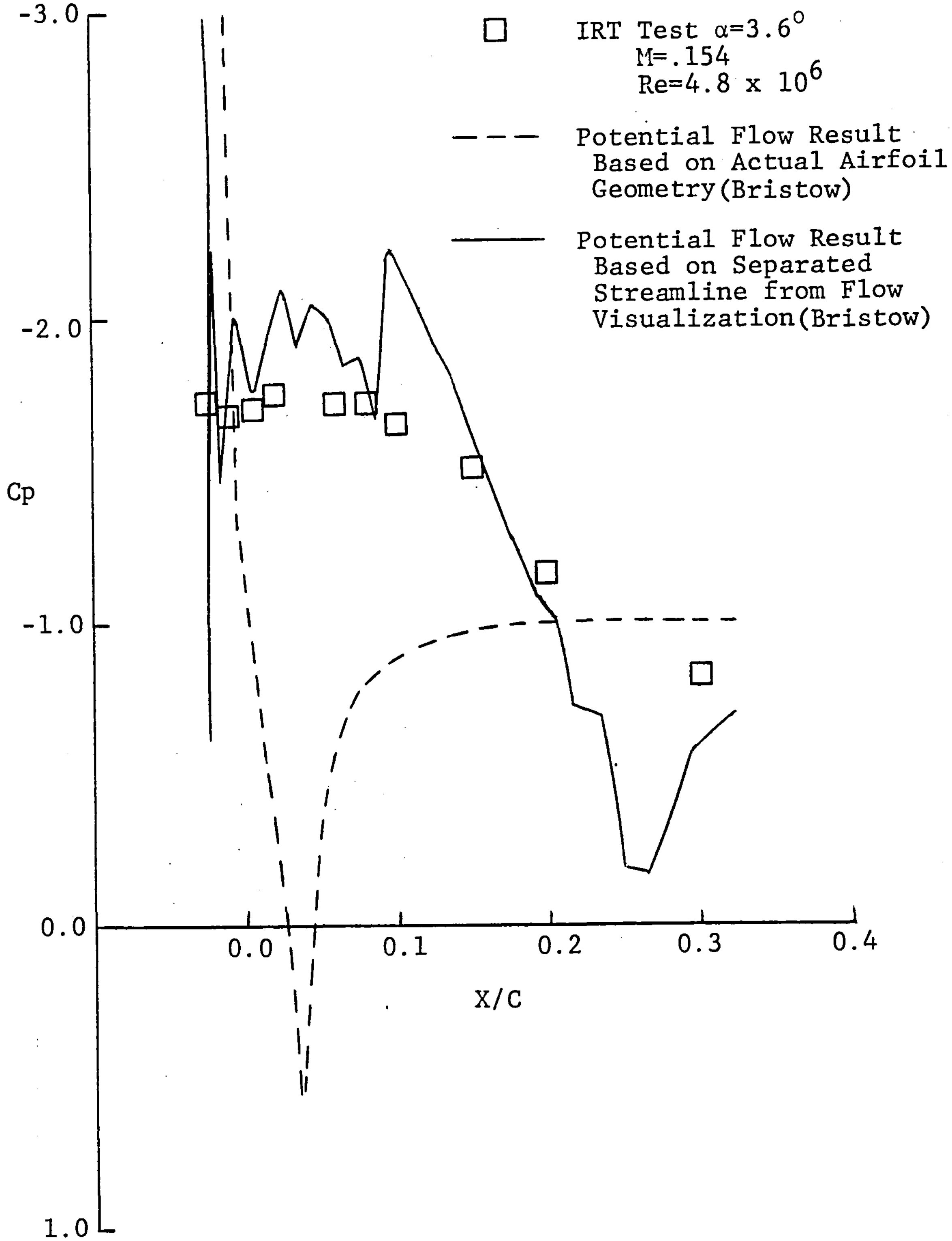

FIGURE 34. PRESSURE DISTRIBUTION IN SEPARATED ZONE BEHIND UPPER SURFACE HORN OF GENERIC ICE SHAPE

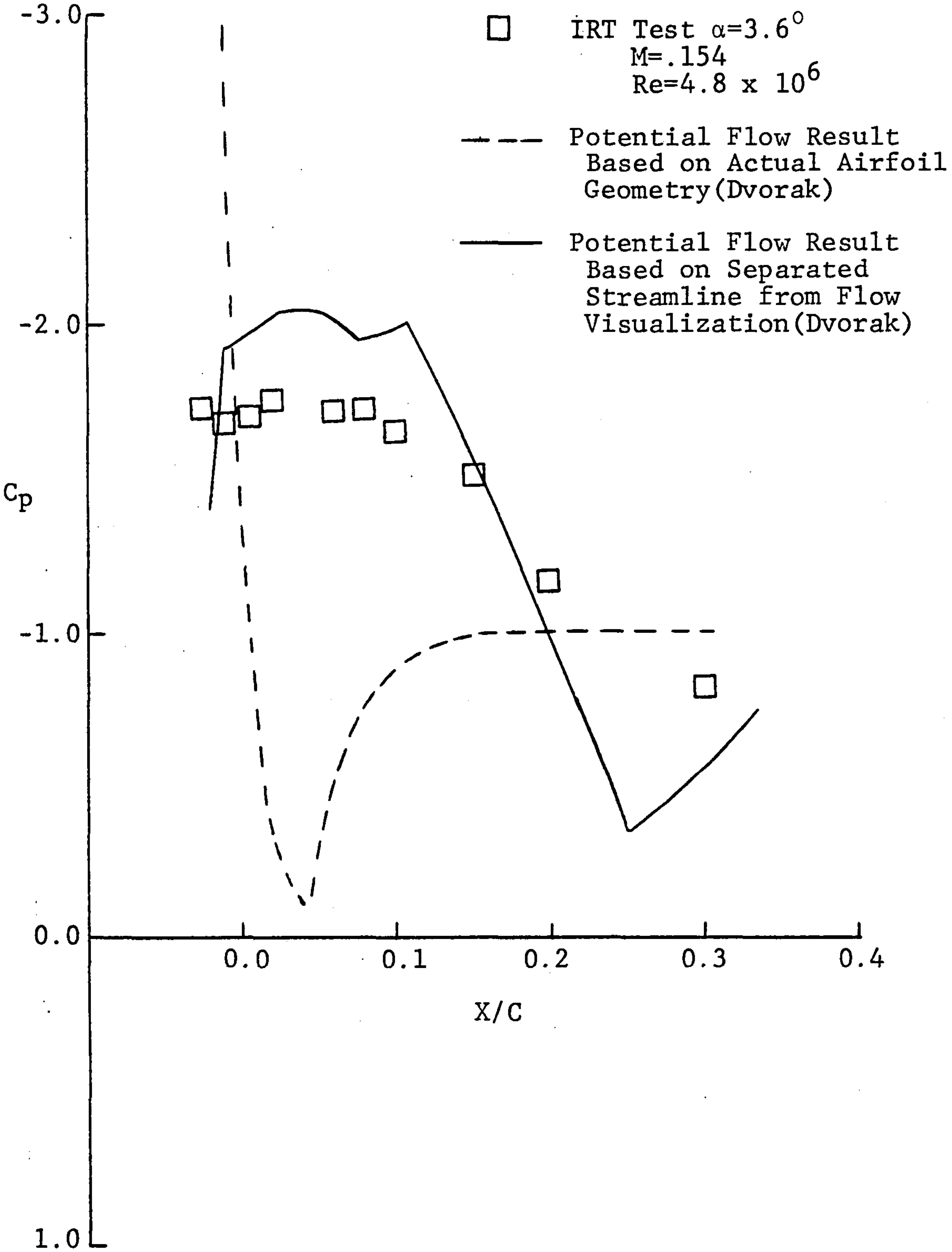

FIGURE 35. PRESSURE DISTRIBUTION IN SEPARATED ZONE BEHIND UPPER SURFACE HORN OF GENERIC ICE SHAPE

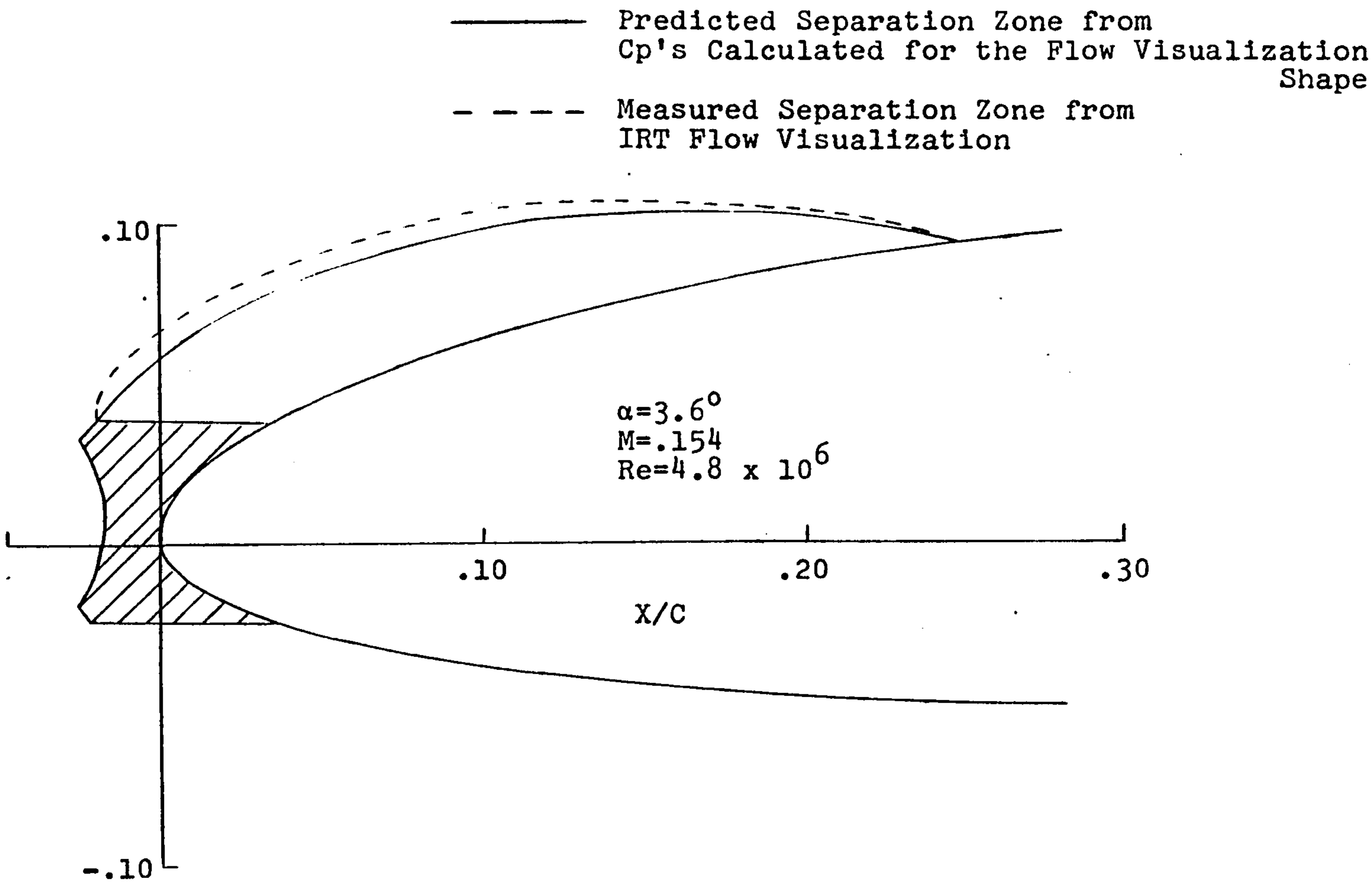

FIGURE 36. EVALUATION OF BRISTOW DESIGN METHOD

1. Report No.	2. Government Accession No.	3. Recipient's Catalog No.
NASA CR-168282		

4. Title and Subtitle	5. Report Date
Potential Flow Analysis of Glaze Ice Accretions on an Airfoil	January 1984
	6. Performing Organization Code

7. Author(s)	8. Performing Organization Report No.
Ronald J. Zaguli	None
	10. Work Unit No.

9. Performing Organization Name and Address	11. Contract or Grant No.
The Ohio State University Dept. of Aeronautical and Astronautical Engineering Columbus, Ohio 43210	NAG3-28
12. Sponsoring Agency Name and Address	13. Type of Report and Period Covered
National Aeronautics and Space Administration Washington, D.C. 20546	Contractor Report
	14. Sponsoring Agency Code 505-45-02

15. Supplementary Notes

Final report. Project Manager, Robert J. Shaw, Propulsion Systems Division, NASA Lewis Research Center, Cleveland, Ohio 44135.

16. Abstract

The results of an analytical/experimental study of the flow fields about an airfoil with leading edge glaze ice accretion shapes are presented. Tests were conducted in the NASA Icing Research Tunnel to measure surface pressure distributions and boundary layer separation-reattachment characteristics on a general aviation wing section to which was affixed wooden ice shapes which approximated typical glaze ice accretions. Comparisons were made with predicted pressure distributions using current airfoil analysis codes such as Eppler and Smetana et al. as well as the Bristow mixed analysis/design airfoil panel code. The Bristow code was also used to predict the separation-reattachment dividing streamline by inputting the appropriate experimental surface pressure distribution.

17. Key Words (Suggested by Author(s))	18. Distribution Statement
Airfoil ice accretion Glaze ice flowfield visualization Potential flow analysis	Unclassified - unlimited STAR Category 02

19. Security Classif. (of this report)	20. Security Classif. (of this page)	21. No. of pages	22. Price*
Unclassified	Unclassified	87	A05

*For sale by the National Technical Information Service, Springfield, Virginia 22161

National Aeronautics and
Space Administration

Washington, D.C.
20546

Official Business

Penalty for Private Use, $300

SPECIAL FOURTH CLASS MAIL
BOOK

LANGLEY RESEARCH CENTER
3 1176 00513 4698

U.S. MAIL

Postage and Fees Paid
National Aeronautics and
Space Administration
NASA-451

NASA

POSTMASTER: If Undeliverable (Section 158
Postal Manual) Do Not Return